Bruna Costa Leopércio

Kinetics of cyclopentane hydrate formation - an interfacial rheology study

DISSERTAÇÃO DE MESTRADO

DEPARTAMENTO DE ENGENHARIA MECÂNICA

Programa de Pós-Graduação em Engenharia Mecânica

Rio de Janeiro
July 2016

Pontifícia Universidade Católica
do Rio de Janeiro

Bruna Costa Leopércio

Kinetics of cyclopentane hydrate formation - an interfacial rheology study

DISSERTAÇÃO DE MESTRADO

Thesis presented to the Programa de Pós-Graduação em Engenharia Mecânica of the Departamento de Engenharia Mecânica PUC–Rio as partial fulfillment of the requirements for the degree of Master em Engenharia Mecânica.

Advisor : Prof. Paulo Roberto de Souza Mendes
Co–Advisor: Prof. Gerald G. Fuller

Rio de Janeiro
July 2016

Pontifícia Universidade Católica
do Rio de Janeiro

Bruna Costa Leopércio

Kinetics of cyclopentane hydrate formation - an interfacial rheology study

Thesis presented to the Programa de Pós-Graduação em Engenharia Mecânica of the Departamento de Engenharia Mecânica PUC–Rio as partial fulfillment of the requirements for the degree of Master em Engenharia Mecânica.

Prof. Paulo Roberto de Souza Mendes
Departamento de Engenharia Mecânica — PUC–Rio

Prof. Mônica Feijó Naccache
Departamento de Engenharia Mecânica — PUC–Rio

Dr. Flavio Barboza Campos
Petrobras

Prof. Márcio da Silveira Carvalho
Coordinator of the Centro Técnico Científico da PUC–Rio

Rio de Janeiro, July 12th, 2016

Bruna Costa Leopércio

Bruna Costa Leopércio graduated in Mechanical Engineering at PUC–Rio in 2014. Soon after, she started to work as an engineer in the Rheology Group (GReo) at PUC–Rio, where she was already involved in research activities as an undergraduate student.

Bibliographic data

Leopércio, Bruna Costa

Kinetics of cyclopentane hydrate formation - an interfacial rheology study / Bruna Costa Leopércio; advisor: Paulo Roberto de Souza Mendes; co–advisor: Gerald G. Fuller. — 2016.

71 f. : il. color. ; 30 cm

Dissertação (mestrado) - Pontifícia Universidade Católica do Rio de Janeiro, Departamento de Engenharia Mecânica, 2016.

Inclui bibliografia.

1. Engenharia Mecânica – Teses. 2. Hidratos. 3. Ciclopentano. 4. Reologia. 5. Reologia interfacial. 6. Interfaces. I. de Souza Mendes, Paulo Roberto. II. Fuller, Gerald G.. III. Pontifícia Universidade Católica do Rio de Janeiro. Departamento de Engenharia Mecânica. IV. Título.

CDD: 621

Acknowledgments

First, I would like to thank my adviser and my coadviser, Paulo Roberto de Souza Mendes and Gerald Fuller. Paulo, not only for his guidance and support, but also for the partnership along the last years, and Gerry for his valuable suggestions and enthusiasm about this research. It was an honor and a pleasure to work with both of you and to participate in such enriching discussions during this time. I learned a lot from you!

Agradeço também ao CNPq e à PUC-Rio pelo suporte financeiro.

Ao Alexandre, Márcio e Bruno pela ajuda na confeção e manutenção da geometria utilizada em todos os testes, sempre com muito bom humor e boa vontade.

Ao pessoal do GReo pela companhia, assistência e risadas diárias. Em especial ao Ricardo, principalmente pela ajuda com o Solid, à Aline pelas dicas do Gnuplot e do Latex, à Priscilla pela bagagem transmitida sobre reologia interfacial e à Alexandra pelos conselhos e ensinamentos sobre reologia passados desde a minha graduação.

Aos meus avós, Myriam e Roberto, pelas quartas-feiras de descanso, que me inspiraram a cada semana.

Ao Ian por me passar às vezes a calma, às vezes a animação que eu tanto precisei e pelas ajudas de toda hora.

Ao meu pai, Waldir, meu porto seguro, por todo cuidado e carinho e ao Lucas e ao João por estarem sempre presentes. A torcida de vocês e a certeza constante de que tudo vai dar certo são estimulantes.

Finalmente, à minha mãe, Christine, por ser tudo que eu preciso, sempre.

Abstract

Leopércio, Bruna Costa; de Souza Mendes, Paulo Roberto; Fuller, Gerald G. **Kinetics of cyclopentane hydrate formation - an interfacial rheology study**. Rio de Janeiro, 2016. 71p. MSc Thesis — Departamento de Engenharia Mecânica, Pontifícia Universidade Católica do Rio de Janeiro.

Hydrate formation and dissociation processes are of major interest in environmental and energy fields. Specifically for the oil and gas industry, hydrate appears as an issue regarding flow assurance, pushing even more the urgent need for expanding the knowledge on hydrate phenomena. In the current work, a new approach to observe and understand the kinetics and mechanical properties of hydrates by interfacial rheology is presented. The standard du Nouy ring is employed with a novel brass cell designed to permit the necessary temperature management. Cyclopentane is used as hydrate former. With the new interfacial geometry, different temperature and water/cyclopentane contact protocols are explored. The importance of first contacting CP against ice crystals in order to initiate hydrate formation is of particular interest. Thus, time sweeps are performed in two stages: one for ice formation and another for hydrate formation. It was determined that cyclopentane hydrates only arise at temperatures $T_f \leq 6^{\circ}$C. A worthwhile discussion regarding the hydrate metastability state is then presented. After hydrates completely populate the water/cyclopentane interface, strain sweeps of the interfacial elastic and viscous moduli (G' and G'') are conducted to examine the fragility of the hydrate films. The mechanical properties of hydrate films demonstrated high dependence on temperature (T_f): the induction time (t_c), measured from the moment when cyclopentane first contacts ice, as well as the elastic modulus (G') and the yield strain (γ_y) increase as T_f is increased.

Keywords

Hydrates; Cyclopentane; Rheology; Interfacial rheology; Interfaces.

Resumo

Leopércio, Bruna Costa; de Souza Mendes, Paulo Roberto; Fuller, Gerald G. **Cinética da Formação de Hidrato de Ciclopentano - um Estudo da Reologia Interfacial**. Rio de Janeiro, 2016. 71p. Dissertação de Mestrado — Departamento de Engenharia Mecânica, Pontifícia Universidade Católica do Rio de Janeiro.

Os processos de formação e de dissociação de hidratos são de grande interesse nas áreas ambiental e energética. Especificamente para a indústria de petróleo e gás, o hidrato aparece como um empecilho à garantia de escoamento, alavancando ainda mais a necessidade urgente de ampliar o conhecimento sobre seus fenômenos. Neste trabalho, uma nova abordagem para observar e compreender a cinética e as propriedades mecânicas de hidratos por meio da reologia interfacial é apresentada. O conhecido anel du Nouy é empregado com uma nova célula de latão projetada para permitir o necessário gerenciamento da temperatura de teste. Ciclopentano é utilizado como formador de hidrato. Com a nova geometria interfacial, diferentes temperaturas e protocolos de contato água/ciclopentano são explorados. A importância de primeiro provocar o contato do CP com cristais de gelo a fim de iniciar a formação de hidrato é de particular interesse. Assim, *time sweeps* são realizados em duas etapas: uma para a formação de gelo e outra para os formação de hidrato. Foi determinado que os hidratos de ciclopentano são detectados em temperaturas $T_f \leq 6^{\mathrm{o}}\mathrm{C}$. Uma interessante discussão a respeito do estado de metaestabilidade dos hidratos é, então, apresentada. Depois que os hidratos preenchem completamente a interface água/ciclopentano, *strain sweeps* são realizados para examinar a fragilidade dos filmes de hidrato, medindo os módulos interfaciais elástico e viscoso (G' e G''). As propriedades mecânicas desses filmes demonstraram uma forte dependência da temperatura (T_f): o tempo de indução (t_c), medido a partir do primeiro contato do ciclopentano com gelo, bem como o módulo elástico (G') e a deformação de escoamento (γ_y) aumentam conforme T_f é aumentada.

Palavras–chave

Hidratos; Ciclopentano; Reologia; Reologia interfacial; Interfaces.

Contents

List of Figures

1
Introduction

1.1
Motivation

In the last decades, hydrates have appeared both as a potential asset and as an issue in various ways. Positively, they have been studied as an alternative source of energy once the amount of energy in each hydrate unit is much more than enough to support its own combustion [4]. As shown in the US Geological Survey map (Fig. 1.1), methane hydrates are widely distributed throughout the globe. Some of the reserves are conveniently located in the coasts of countries such as Japan, South Korea and Chile which do not have significant conventional natural gas reserves. Indeed, this strengthens the interest in developing viable ways of commercially exploiting this unconventional gas resource. Estimates suggest that those deposits have at least twice the quantity of energy of all fossil fuel reserves available worldwide [5].

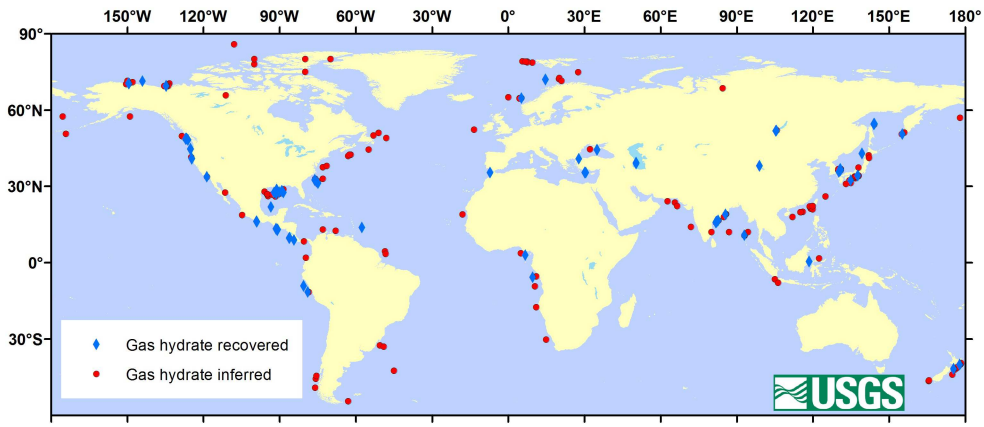

Figure 1.1: Map of locations where gas hydrate has been recovered (blue diamonds) and inferred (red circles), from US Geological Survey.

Other technological application is the use of hydrates to desalinate seawater. The viability of this separation technique is not guaranteed yet but it can be a fruitful development to many countries [5], especially given the limited sources of freshwater and the high growth rate of human population. Another separation

process under investigation is the one employing hydrates to extract CO_2 from flue gas exhausted by large power plants [6] in an attempt of reducing carbon emissions and mitigate climate change and global warming.

Natural gas storage and transportation by hydrate is also being explored. The rising demand for natural gas stimulates the development of alternatives to store and supply natural gas to different regions. Despite loading less amount of gas per cubic meter when compared to the conventional transporting technologies, such as LNG (liquefied natural gas) and CNG (compressed natural gas), that method presents advantages since it does not involve cryogenic temperatures or the high pressures of cylinders [7, 8].

All these possible applications and the lack of effective methods to make them viable on massive scales are more than enough to justify the global mobilization to further investigate hydrate phenomena. Nonetheless, some imminent negative aspects have propelled even more the capital raising directed to knowledge development on hydrates.

The extreme risk of gas hydrate blockages in pipeline and offshore facilities, once the conditions in deep sea waters are proper to hydrate formation is of great concern. It can compromise facility safety, damage equipment, harm the marine environment and put personnel in safety hazard [6]. Indeed, there are registers of hydrate plugs (Fig. 1.2) as well as accidents caused by them. Consequently, huge investments are made by the oil industry in order to prevent or manage hydrate formation. The results include the development of some processes to ensure regular flow, namely chemical, hydraulic, thermal and mechanical [6]. All of them representing considerable increase in production costs. This may have been the greatest driving force propelling hydrate investigation over the last years. Most of the companies have chosen to work with risk management instead of avoidance. Since kinetics enables the management, it is essential to quantify it [9].

Figure 1.2: Gas hydrate plug recovered from a subsea pipeline off the coast of Brazil (courtesy of Petrobras).

Besides a possible underwater blowout during drilling, the more serious issue of in-situ hydrates is regarding global warming. Figure 1.3 illustrates a possible "negative feedback" scenario featured for some researchers that could create a "runaway" greenhouse effect. Methane is a strong green-house gas, with a global warming potential greater than that of carbon dioxide. Thus, earth's temperature rise could cause decomposition of the methane in natural deposits which would imply in enhancement of global warming which, in turn, would cause more methane release [1].

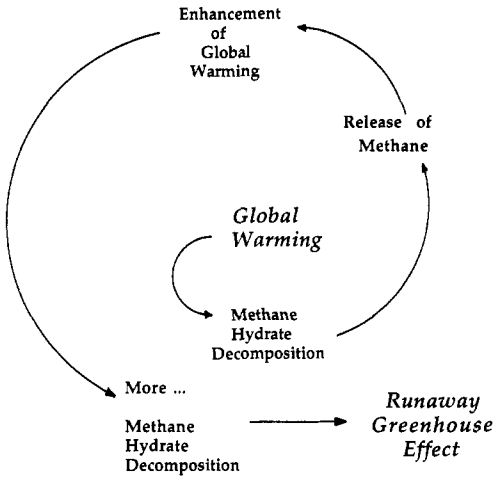

Figure 1.3: Runaway greenhouse effect scenario, reproduced from [1].

Therefore, all of these data show a worldwide growing need for a better understanding of hydrates, which would be enough to motivate the present research. Furthermore, even though the comprehension on hydrate thermodynamic is extensive, there is still some lack of knowledge regarding hydrate kinetics [4]. In this sense, we use interfacial rheology as a means of studying the kinetics of the formation process of a cyclopentane hydrate once it starts at the interface between water and the hydrocarbon, as will be seen later.

1.2 Research objectives

The main objective of this thesis is to qualitatively track down the kinetics of hydrate formation, probing the interface between water and cyclopentane, since it is where the nucleation starts. In this regard, a new geometry for interfacial measurements with temperature control is designed and built and a protocol for hydrate forming experiments using this new geometry is established. Meanwhile, some relevant properties of cyclopentane hydrate films are measured.

1.3 Outline

This thesis is divided into four more chapters besides this first one. In Chapter 2 the concepts of interface and interfacial rheology are presented and the state of art is revisited. It points out to the main techniques of rheologically probing interfaces. Still in Chapter 2, the most relevant facts about hydrates are summarized and some relevant concepts (e.g. induction time, dissociation temperature, metastability...) are defined. A long discussion about the existence or not of the memory effect is conducted and some relevant applications are listed. After that, a briefing is made in the literature on cyclopentane hydrates and their main characteristics.

Chapter 3 itemizes the materials used during the tests. The experiment set-up is depicted in detail, including the description of the developed novel brass cell for interfacial measurements. The rheometric experiments are also presented. Then, a correction to account for the torsional strain of the du Nouy ring is formulated. This correction is better explained later in Appendix A, which also integrates this chapter.

Following, Chapter 4 presents the results of the rheological measurements. Data for time sweeps (Sec. 4.1) and strain sweeps (Sec. 4.2) are exhibited. Some comparisons between the results obtained under different temperatures are made and a tendency for the interfacial elastic modulus, the critical time and the interfacial yield strain can be observed.

Finally, Chapter 5 brings the main conclusions of the present research as well as some suggestions for future works.

2
Background and Literature

2.1
Interfacial Rheology

Rheology is the study of the deformation and flow of matter in general, and rheometry is the rheological property measurement. Commonly the main interest is in materials with characteristics between those of ideal liquids and solids. So, rheometers are usually used for measuring bulk or three-dimensional properties of these materials. However, at the interface between two immiscible liquids or between a liquid and a gas there is a two-dimensional phase with distinct rheological attributes [2, 10].

Interfaces can be deformed by changing their area - dilatational deformation - or by moving its elements relative to each other - shear deformation, as shown in Fig. 2.1 [2, 11–14].

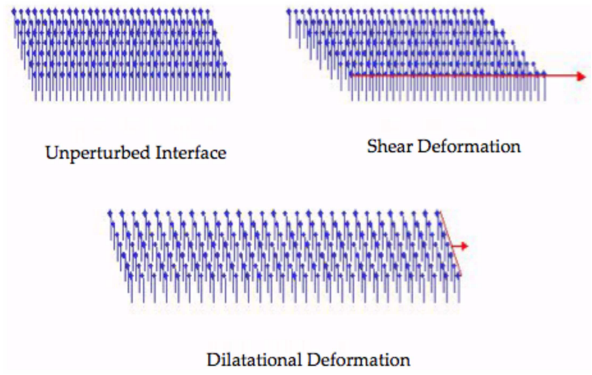

Figure 2.1: Interface deformation, replicated from [2].

Generally, interfacial rheology describes the functional relationship between the deformation of an interface, the stresses exerted in and on it and the resulting flows in the adjacent fluid phases. For each deformation type - shear and dilatational - there are distinct interfacial rheological parameters. The interfacial shear viscosity is defined as the ratio between the shear stress and the shear rate in the plane of the interface: $\eta_s = \sigma/\dot{\gamma}$, whereas the interfacial dilatational viscosity is the uniform expansion of the interface at a constant rate: $\eta_d = d_\gamma/d(lnA)dt$ [15].

Viscoelastic characteristics of the interface can also be measured. In oscillatory experiments, for example, the strain or stress is sinusoidally varied at an angular frequency while the storage and the loss moduli (G' and G'') are acquired. The storage modulus represents the energy stored during stress and the loss modulus represents the energy that is lost during sample loading [15].

As well as the bulk viscosity, the interfacial viscosity depends on the pressure, temperature, shear rate and time, among other factors. Interfacial measurements are not easily acquired because of several reasons: (1) interfaces are very delicate, and generate small torques; (2) the contributions of the sub-phases must be minimal; (3) the geometry of the interface should give uniform shear and quantitative interfacial viscosity and modulus values and, finally, (4) the geometry must be easily positioned at the interface.

Over the past few decades, different techniques were developed to characterize interfacial properties and can be classified in indirect and direct methods. In indirect techniques, tracer particles are placed at the interface and their displacement is tracked by image. In a general basis, they are restricted to the gas/liquid interface. In direct techniques, the displacement (torque) of a probe at the interface is directly measured. The classical instruments used in this method are basically composed of a circular measuring body that touches the interface of a liquid suspended from a thin torsion wire [16].

Different apparatus for indirect measurements, such as the channel surface viscometer, the deep channel surface viscometer, the rotating knife-edge in wall surface viscometer and the transient rotating cylinder apparatus, as well as some for direct measurements, such as the Wilhelmy plate, the magnetic-rod rheometer, the bi-cone geometry and even a 2D micro-rheology technique, have been used [14–19]. However, some disadvantages taint the accuracy of these methods, mainly on account of the low forces and torques involved and the complex relation between the interface and the bulk of the fluid [14, 17].

The du Nouy ring is a standard device for surface/interface tension measurements that can be used either in a viscometer or in a rheometer. Its light framing permits the characterization of fragile interfaces. Nevertheless, some rheometers have very low sensitivity to use the du Nouy ring in oscillation mode.

In 2009, Fuller et al. [20] presented a double-wall-ring geometry to measure the viscoelastic properties of interfaces in shear flows, which is a 2D equivalent of a double wall Couette setup. It comprises a cylindrical chamber configured to retain a fluid therein, an inner cylinder concentric with an axis of the cylindrical chamber and a ring that can have various cross section shapes. The double-wall-ring was designed to yield an average shear rate in the inner region that is the same as an average shear rate in the outer region. An embodiment of their invention

was reported by Vandebril et al. [17] and consists on a ring bigger than the du Nouy with a diamond cross section and a trough. Nevertheless, many variations and modifications of the assembly described are apparent and some of them are already commercialized, including a double wall du Nouy ring.

Recently, the interest in interfacial rheology has risen. Most of the applications are associated with emulsification processes and stability of emulsions and suspensions due to its importance to several industries including petroleum, cosmetics, pharmacy and food production [21–26]. Apart from that, some studies have acknowledged that interfacial rheology plays a key role in biological processes [14]. The membrane of living cells, for example, is formed from phospholipid bilayers and define an interface between two regions of essentially the same fluid [26, 27].

2.2 Hydrates

Hydrates are composed of hydrogen-bonded water molecules and a guest (gas or liquid) molecule entrapped in their center. These two components are not chemically connected [1, 28] but, under appropriate thermodynamic conditions, they form a crystalline solid compound physically similar to ice that, in most cases, ignite when lit. This solid compound is stabilized by van der Waals forces. Unlike the inorganic hydrates, the gas ones are nonstoichiometric [5, 8, 29–31].

Fig. 2.2 shows a simplified hydrate phase diagram, which indicates the temperature and pressure region for stable hydrate formation. The blue curve indicates the condition at which hydrates dissociate to release the two former agents. Each guest molecule provides a different phase diagram, but usually, low temperatures and high pressures are needed.

The phase diagram of many gas hydrates have been mapped out. In general, lower molecular weight gases such as methane and carbon dioxide require higher pressures and lower temperatures to form stable hydrates (methane forms a stable hydrate at 4^{o}C when the pressure reaches 3.9 MPa, for example), whereas hydrocarbons such as propane require less severe conditions. Apart from that, some compounds such as tetrahydrofuran (THF) and cyclopentane (CP) form hydrates at atmospheric pressure [32].

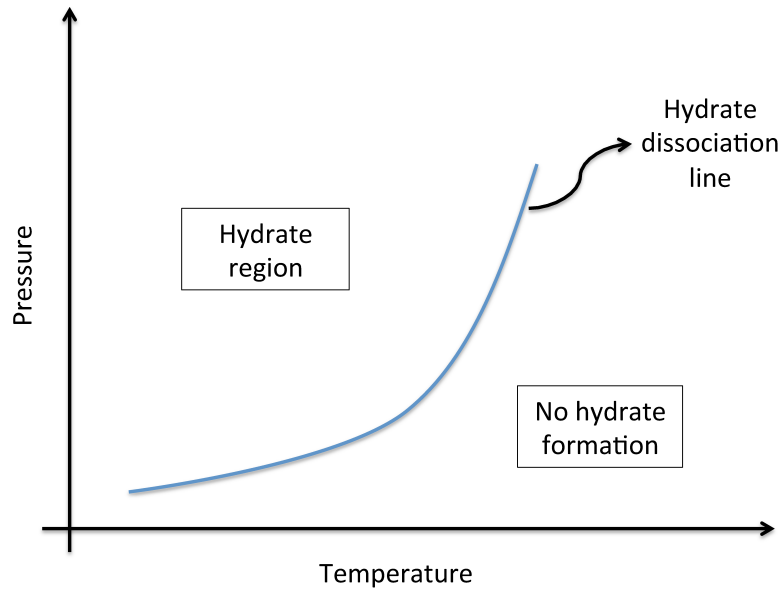

Figure 2.2: Simplified hydrate phase diagram: hydrate formation requires high pressures and low temperatures.

2.2.1 Hydrate structures

There are three most common crystalline structures of hydrates, classified by the nature and size of the guest molecule: structure I, structure II and structure H (see Fig. 2.3). They are formed by convex polyhedrons connected through their vertices, face-sharing in three dimensions or through face-sharing in two dimensions to form the hydrate structures. These structures are the smallest crystal unit that repeats itself in space [30].

Type I hydrates (Fig. 2.3(a)) normally sequester small hydrocarbon molecules, such as methane, ethane and carbon dioxide. They are found mainly in nature [28]. Type II hydrates (Fig. 2.3(b)) generally trap larger molecules, such as propane and isobutane, and are commonly found inside gas and oil pipelines. Type H hydrates (Fig. 2.3(c)), in turn, usually contains a combination of at least two different guests: isopentane or neohexane accompanied by smaller molecules such as methane, hydrogen sulfide, or nitrogen [30, 33].

The guest molecules are able to rotate inside the cages and also to distort them, but they cannot diffuse between the cages. It is interesting to note that not all the cavities need to be occupied for the guest molecules. The occupancy is directly related to the guest size and to the pressure, temperature and composition of the system [3]. In structure H, the shape of the guest molecule is also relevant [30].

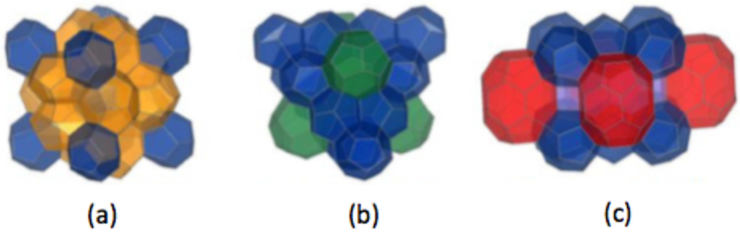

Figure 2.3: Hydrate crystalline structures: (a) I, (b) II and (c) H (modified from [3]).

All ideal fully occupied hydrate structures are formed of about 85 mole % water and 15 mole % gas. Moreover, both ice and hydrate crystal structure consists of water molecules hydrogen-bonded in a solid lattice. Because of that, despite some exceptions, such as yield strength, thermal expansivity and thermal conductivity, most of hydrate properties are similar to ice [30]. Both of them possess a good metal adhesion and density lower than water and higher than most of oils.

Nevertheless, the formation process of hydrate is different from ice. While ice formation is a bulk phase change of water (from liquid to solid) [8], a number of researchers have confirmed that hydrates are formed at the hydrocarbon/water interface, as will be discussed later [34–38].

2.2.2 Hydrate formation

There are two phases during hydrate formation process: nucleation and growth. Nucleation is a microscopic process during which small water and gas agglomerates emerge and disperse to achieve a critical size for continued growth [30, 39]. It is influenced by a lot of parameters: displacement from equilibrium conditions, surface area, agitation, water history and gas composition. Therefore, it is considered a stochastic process. Some studies reported that data spreading is even more significantly when low driving forces and isothermal conditions are involved [30, 40–42].

If the critical size is not reached, the small crystalline structures melt, characterizing a metastable state. Thus, between the two regions shown in Fig. 2.2, separated by the dissociation curve (or hydrate phase boundary), there is a third one called the “hydrate metastability zone” (see Fig. 2.4) in which gas and liquid water begin to rearrange into the orderly hydrate crystal structure [30, 31]. Because entropy favors disorder over order, this process can last seconds or hours. The time elapsed during the entire nucleation process is called induction time. Practically, the induction time also includes the onset of growth up to the point at which hydrates are first macroscopically detected since nucleation occurs on a too small size scale

to be detected.

Two important concepts that influence a lot the kinetics of hydrate formation and the rate of reaction are the subcooling and the overpressure. The first is defined as the difference between the temperature at which dissociation and formation happens. The second, in turn, is defined as the difference between the experimental pressure required for hydrate formation and the hydrate stability pressure when both are measured at the same temperature. The induction time varies with the subcooling and the overpressure in the system: the higher they are, the lower is the induction time [30, 31, 43].

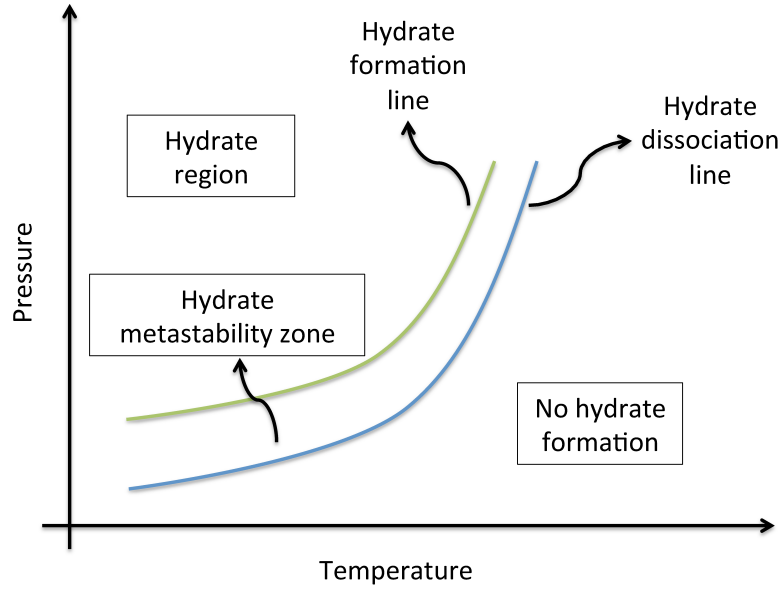

Figure 2.4: Hydrate metastability zone.

Multiple researches have evidenced that hydrate nucleation happens at the interface between water and hydrocarbon, where the Gibbs free energy of nucleation is lower. It is explained by the very high concentrations of both hydrate components at this site and the mutual insolubility at low concentrations of hydrocarbons and water [28, 38, 44–46].

Nowadays, there are basically two conceptual molecular models of hydrate nucleation at the interface: the labile cluster hypothesis and the local structuring hypothesis. In the labile cluster hypothesis, liquid water molecules are considered to be arranged around a dissolved solute molecule in a “prehydrate” structure. However, the large free energy that needs to be overcome during this mechanism causes criticism [47]. Thus, a modification of this hypothesis is based on adsorption and clustering on the vapor side of the interface. In the local structuring hypothesis, the guest molecules are ordered in configurations similar to that of hydrates [30]. Nevertheless, there is still lack of experimental verification on both hypotheses.

In turn, hydrate growth experiments are more tenable. This phase occurs after nuclei have achieved a critical size at any temperature below the hydrate dissociation temperature (the maximum temperature at a specific pressure above which no hydrates arise - see Fig. 2.4). During growth, mass and heat transfer become of major importance together with the nucleation parameters cited above [30].

Over the years, the scientific community has pointed out the existence of a "memory effect" that reduces the induction time, and, consequently, accelerates a new hydrate appearance. Two major reasons have been proposed to explain this phenomenon [30, 38, 45, 48–52]. The first and oldest one is the presence of some sort of residual molecular structures in the aqueous phase that can persist for a long time after dissociation, being transformed in nucleation sites when cooled again. It usually happens when the temperature for melting hydrate is close to the dissociation temperature or insufficient time is given to melt hydrate. The second one is the remaining dissolved hydrate-forming component in solution after hydrate melting due to a supersaturation of the guest component. Additionally, impurities such as silica, rust and clay, are also considered reducers of hydrate induction time [8], as well as turbulent conditions of flow. Nonetheless, there has not been a general consensus that hydrates retain a "memory".

In 2000, Takeya et al. [45] dissolved CO_2 in water under pressure to analyze the freezing-memory effect. Their experiments showed that the nucleation rates significantly increase when the water is previously frozen as ice and melted, but only if the heat provided to melt water is not too high (below 298 K). They suggested that it happens exactly due to clathrate-like structures that remain in solution.

In 2002, Kaschchiev and Firoozabadi [53] developed a general formula for the driving force of hydrate crystallization which they identify as the supersaturation, sensitive to the conditions of gas in solution.

Results showing that cyclopentane hydrates could be formed faster if a small amount of dissociated cyclopentane water solution is added to the system than using the system with no hydrate history alone were presented by Sefidroodi et al. [52] in 2013.

A year later, Zylyftari et al. [38] used a small quantity of ice to trigger hydrate nucleation and growth on an emulsion. They compared the results of an ice-forming emulsion with isooctane (which does not form a hydrate structure) to a hydrate-forming emulsion with cyclopentane. According to the authors, cyclopentane hydrate is heterogeneously nucleated by ice at the ice-organic-aqueous contact line and ice seeding is less effective than hydrate seeding.

Sowa and Maeda [48], in turn, used a high pressure automatic lag time apparatus (HP-ALTA) to test the memory effect in ethane-propane mixed gas

hydrates by four different boats. They concluded that the memory effect do exist, but its amount varied among the boats. Their results do not sustain one of the existing hypotheses for the memory effect existence alone, but a combination of them.

On the other hand, the high pressure automatic lag time apparatus was also used by Wilson and Haymet [54] to study THF-water hydrate formation. They claim that probably, the previously reported instances of memory effect are due to the inherent stochastic nature of heterogeneous nucleation and to the small amount of runs on the same sample of the protocols. Thereby, the meaningful statistics do not become evident.

Prior to that, Buchanan et al. [55], in 2005, analyzed the structure of water before hydrate formation and after hydrate decomposition and could not determine any significant difference in the water structure itself nor in the water around the methane, suggesting that the memory effect does not exist.

2.2.3 Hydrate dissociation

Hydrate dissociation is an endothermic process that consists on supplying external heat to break the hydrogen bonds between water molecules and the van der Waals interaction forces between the guest and water molecules of the hydrate. However, a finite driving force is required.

In contrast to hydrate formation, the dissociation is a repetitive process that can be reproduced if the experiment is careful. This happens because the gas and liquid phases are disorderly and consequently favored by entropy. So, after hydrate being removed from the temperature and pressure stability region, dissociation begins rapidly, unlike formation which is hindered by the metastable period (see Fig. 2.4). In fact, this is the reason why there is a substantial difference in hydrate formation and dissociation points [30, 31].

Hydrate inhibition techniques have been on focus since the 1940s and 1950s when some researches studied the inhibitory effects of chloride salts of calcium, sodium, and potassium along with methanol and monoethylene glycol [30, 56, 57]. By then, a lot of progress was made into this matter, including the development of depressurization, thermal stimulation and thermodynamic inhibitor injection techniques. In the 1990s, chemicals inhibitors were introduced as substitutes of the traditional thermodynamic inhibitors (e.g. methanol, ethanol, glycols). They are called low-dosage hydrate inhibitors (LDHIs) and generally fall into two classes as kinetic inhibitors (KHIs) and anti-agglomerants (AA). The objective of using thermodynamic inhibitors is to change the hydrate “envelope” so that the pressures and temperatures of the system become outside of it. The KHIs, in turn, delay the crystallization time whereas the AAs make hydrate particles remain dispersed to avoid

agglomerates [28, 30]. Nowadays, the industry has favored hydrate management technics, with anti-agglomerants for example, instead of hydrate avoidance technics, with inhibitors. This means that it is essential to quantify hydrate formation kinetics and flow properties once risk management is enabled by kinetic [9].

Surfactants have also been studied by several researchers, both as hydrate promoters [58] and as anti-agglomerants [59, 60]. However, the approaches used in these studies were applied to water in contact with hydrate formers (natural gas [58], THF [59] and cyclopentane [60]) subjected to agitation. However, the convection associated with agitation is expected to strongly affect the kinetics of hydrate formation since this rate is expected to be a balance of convection, diffusion, and intermolecular forces [61]. An uncontrolled agitation makes it difficult to assess the surfactant effect on agglomeration [59, 60] .

2.2.4 Hydrate benefits and drawbacks

Due to the proper conditions, gas hydrates are particularly prevalent in polar regions and deep sea. In polar regions, they are found onshore and offshore, while in deep sea waters they are found in the outer continental margins [62], where there are massive reservoirs of methane. Indeed, not only the global volume of hydrate-bound gas is large, but also some individual gas hydrate accumulations may contain significant and concentrated resources that may profitably be recovered in the future. Consequently, hydrates are regarded as a future energy resource [4, 6, 63–65], particularly for countries that do not have significant conventional natural gas reserves.

In addition, hydrates are potential mediums of gas storage and gas transportation. For this reason, some attention has been paid to their use as a means of safely storing hydrogen and natural gases [1, 65–67]. In the former case, this application is more suitable for stranded gases that are too small to justify a liquefaction facility and too far away from a pipeline [5, 68]. Apart from that, this storage technology can be considered safer than the storage in the usual high pressure cylinders for metastable gases at atmospheric pressure and low temperatures (e.g. methane) [8]. Hydrogen was first thought to be too small to form stable hydrates, but some studies demonstrated that they can surely form structure II at pressures greater than 200 MPa at room temperature [69, 70].

It is also possible to use hydrates to separate gases from a gas mixture. Under high pressures and low temperatures, the non hydrate-forming gas can be captured as a solid. It can be applied to flue gases in order to selectively capture harmful gases, such as dioxide carbon, while excluding nitrogen and other benign gases for example [5, 6, 66]. Yet, finding mechanisms to reduce the pressure required to form

hydrate is still necessary in order to decrease the embedded costs [71–73].

Apart from that, desalination of seawater using hydrates is under investigation. The process starts with brine being mixed with a hydrate former gas. Once clathrate is formed, isolating water from the dissolved solids and salts, it precipitates. After then, the hydrate is heated to release the gas. Thus, the final product is freshwater [74]. The advantages of applying this technique instead of using ice include the temperature operation which is not limited to values below the freezing point of ice [67, 75, 76]. Although the economic and technical feasibility of this process is not certain, it can be very important for the next years since the world population is increasing in high rates and the freshwater supplies are scarce [5, 6, 77].

Hydrates can also be used as a phase change material slurry in the secondary refrigerant loop in cooling systems (i.e. air conditioners and refrigerators) [6, 78–83]. Secondary refrigerants are used to transfer heat from the substance being cooled to a heat exchanger where the heat is absorbed by a primary refrigerant. Due to its high latent heat and thermodynamic stability above ice melting point (0^{o}C), hydrate slurry superimposes itself over some currently used methods: aqueous solutions and ice slurry. However, problems involving hydrate agglomeration in the device are common and jeopardizes its usage [78].

The more pressing need for research into hydrate structures arises from the problems they create regarding flow assurance. In fact, since 1934, when Hammerschmidt [84] first identified gas hydrate formation as the reason for pipeline blockage, the petroleum industry has been concerned about these structures. Hydrates can rapidly develop in offshore and onshore production lines and, in extreme cases, completely block the flow of oil and gas [5, 39]. They can also form during drilling and well completion or during abnormal conditions, such as well tests with water or start-up after a shut-in period. Actually, hydrates represent a more severe problem than other solid precipitations because their appearance rate is higher than the one of waxes and asphaltenes [3]. Moreover, they also compromise facility safety and increase production costs. For example: once hydrates form a plug and a one side depressurization is made, it separates the pipe in a high pressure section upstream, between the well and the plug, and a low pressure section downstream, between the plug and the recovery division. If the difference between the pressures increases, the plug can behave as a projectile that destroys the pipe. Besides, pipe blasts are also possible in the upstream section if high temperatures are involved. These situations can damage equipment and, worse, put personnel in safety hazard [6]. Indeed, there are records of injuries caused by explosions due to hydrate plugs. For those reasons, it is estimated that the petroleum industry spends about one billion US dollars a year to prevent hydrate formation in wells, pipelines and

equipment [63].

In this sense, the aforementioned discussion about the existence or not of the "memory effect" is another major interest to the oil and gas industry. For example, after a first hydrate formation in a pipeline, hydrate dissociation should be accompanied by the removal of the water phase. Otherwise, the residual structure or dissolved gas would enable fast formation of future hydrate plugs. On the other hand, if hydrate formation is desired, it could be promoted by multiple dissociation and reformation experiments [30].

Finally, hydrates are an environmental concern. They appear as a real threat to global climate once methane from reservoirs in the oceans may be released in the atmosphere by decomposition if the sea floor warms up by a few degrees Celsius [62, 65, 85, 86]. This gas is able to absorb more infrared radiation than carbon dioxide, being, on a molecule basis, much more effective as a greenhouse gas than additional CO_2. Besides, its release to the ocean could cause continental slope destabilization and marine ecosystem change [6, 85].

Since the mechanical blockage of transportation lines by hydrates is a primary concern, considerable research activity has been directed toward the flow response or rheology of these structures. The approach that has been invariably used is to create emulsions of water-in-oil that are, in turn, subjected to the presence of hydrate-forming hydrocarbons, and the rheological responses (viscosity, yield stresses, moduli) are measured. In 2012, researchers at the Center for Hydrate Research at the Colorado School of Mines used this strategy on water-in-crude emulsions subjected to pressurized methane and reported that the resulting hydrate-laden mixture was strongly shear thinning [87]. They concluded that the observed non-Newtonian response and associated yield stresses were consequences of a competition between cohesion of hydrate-coated water drops and shear-induced breakdown. More recently, they applied the same methodology but used mineral oil in place of crude oil [88]. This study reported a steep increase in the system viscosity upon the inception of hydrate formation and again observed yield stress behavior following by strong shear thinning.

2.2.5 Cyclopentane hydrates

Cyclopentane (C_5H_{10}), sometimes referred to as CP, is an alicyclic hydrocarbon with 70,1g/mol of molar mass. It forms hydrates at a stoichiometric ratio of 1:17 of cyclopentane to water molecules [89, 90]. It is immiscible in water and forms the cubic hydrate structure II at ambient pressures and at temperatures easily accessible in laboratory, meaning that pressurized experimental environments are not needed. Tests at atmospheric pressure are usually more accessible, cheaper and safer than

the ones involving a pressurization process. Therefore, cyclopentane is often used as a model material in hydrate studies [32, 43, 90–99], including some at PUC–Rio [100–102] with a lot of different applications.

Several researches had measured the dissociation temperature of cyclopentane hydrates formed at atmospheric pressure. Most of them agree that this dissociation temperature is 7.7^{o}C [30, 43, 97, 103].

The hydrate rheology research group at The City College of New York (CCNY) has been investigating the rheology of hydrate systems using emulsions of water-in-cyclopentane. The system they employed, however, was very complex - a blend of cyclopentane, Span 80 surfactant, halocarbon oil, and mineral oil - and was designed to produce a density-matched mixture, which arrested the complication of creaming of the emulsion over time [32]. This study reported large increases in viscosity of the hydrate forming mixtures that were not a strong function of shear rate. Instead, the onset of hydrate formation was mainly a result of subcooling. More recently, they associated the viscosity evolution during hydrate formation in oil-in-water emulsions with the hairy hydrate structure and porosity development that could lead to a jammed state depending on the applied stress [94, 95].

Nakajima et al. [97], in turn, examined cyclopentane-in-water emulsions with surfactants as potential thermal energy storage media for air-conditioning systems by evaluating the heat of dissociation of the formed hydrates. They determined that those emulsions are, in fact, a promising thermal energy-storing material.

Corak et al. [96] research was driven by their interest in improving desalination technologies. CP hydrates thermodynamics and kinetics were investigated. In addition, the effective hydrate number and the purity of the water recovered from the hydrate were assessed. The results pointed that the purification of the water desalinated from a 3 wt.% NaCl brine is better in a high subcooling at atmospheric pressure.

Tohidi et al. [98] compared hydrate forming compounds and concluded that cyclopentane is the strongest hydrate promoter. Nonetheless, Dirdal et al. [43], during their experiments with well-known classes of KHIs using cyclopentane hydrate-forming fluids, found that CP hydrate formation was inconveniently slow if fluids with no hydrate history were used. In this sense, before that, Fan et al. [99] had also reported the need for a long waiting period to form cyclopentane hydrates.

Cyclopentane has been widely applied in many hydrates trials and the results have revealed important information. However, most of the studies rely on bulk rheology measurements of emulsions and thus suffer from a number of limitations. Since the rheology of emulsions depends on the drop size distribution and the mechanical properties of the interfaces (surface tension and interfacial rheology), it can be difficult to obtain reproducible results that can be generalized. The unwanted

contributions from gravitational settling and coarsening of the emulsions must be avoided. At the same time, the addition of surfactants and blends of oils to density-match the liquid pairs unavoidably introduces unwanted interactions in the resulting complex, multicomponent mixtures.

Thus, the present work submits a straightforward approach to investigate the mechanics of hydrate systems in which interfacial rheology is used to directly measure the hydrate film dynamics. It basically relies on the evidences that the interface is the site of hydrate nucleation and subsequent growth. Cyclopentane was chosen as the hydrate former exactly because it is not miscible with water and because it forms hydrates at ambient pressures and easily accessible temperatures.

3
Experiment Set-up and Methodology

Deionized water obtained from a Simquis purifier system and ≥75% pure cyclopentane from Sigma-Aldrich were used to perform all experiments described in this chapter. No preliminary treatment was applied to the materials.

The rheometer employed was the DHR-3 (Discovery Hybrid Rheometer 3) from *TA Instruments*, which is an hybrid rheometer with stress and strain control (Fig. 3.1). It has a Peltier system that provides the temperature control during measurements.

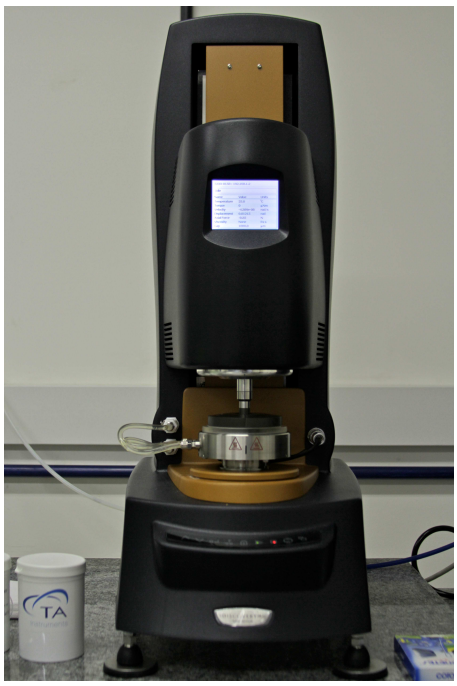

Figure 3.1: Rheometer: DHR-3.

3.1
A novel brass cell

The geometry used to perform all the measurements presented in the next chapter was a modification of the “double wall ring” (DWR) interfacial geometry, which is composed by a ring and a Delrin double wall cell, where the material to be tested is inserted.

In order to follow the development of hydrates, it is essential to control and change the system temperature. In this sense, it was found to be mandatory to design and manufacture a different cell, mainly for two reasons: (1) the standard cell is made of Delrin, which is a highly-crystalline engineering thermoplastic known as a bad thermal conductor that impedes one to impose and control the temperature of the system and (2) the standard cell requires a big amount of fluid for each test, which hampers the temperature control even more.

The modified geometry consists of a brass double wall cell and a du Nouy ring. The du Nouy ring, shown in Fig. 3.2, is a stainless steel geometry with 20mm of diameter and a round cross-section.

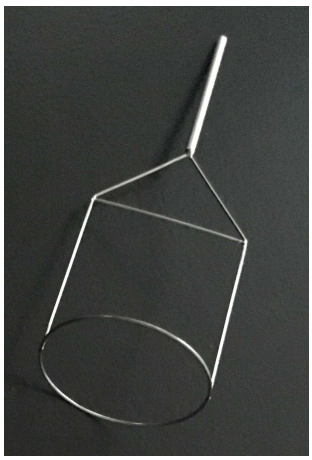

Figure 3.2: Du Nouy ring.

The changes in the material and size of the cell were designed in order to accelerate the heat transfer across the sample. The new cell has dimensions smaller than the standard one, once the trough requires only $\approx$ 1.8 mL of water to be filled (Fig. 3.3). It sits on top of a Peltier plate of a rotational rheometer that is the component responsible for controlling the sample temperature. A fluid chosen by the user flows inside the Peltier plate cooling or heating it in accordance with the command of a platinum resistance thermometer sensor that is positioned at the center of the plate and ensures accurate temperature measurement and control. As brass is a good thermal conductor, the temperature imposed by the Peltier plate can rapidly be transmitted to the rest of the system. This transmission is even faster because of the small amount of sample involved. With these changes, the user is able to impose a temperature to the interface, which was not possible with the old system.

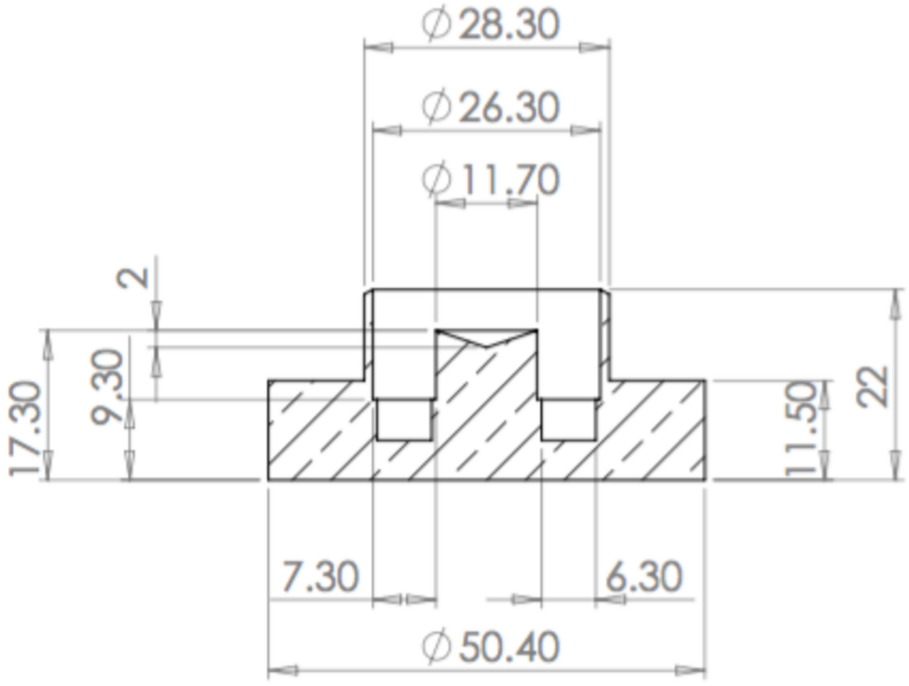

Figure 3.3: Dimensions of the novel brass cell in millimeters.

As well as in the standard cell, there is a step at the inner and outer channel walls of the brass cell marking the height level of the lower fluid (normally water). Details of the new cell can be seen in Fig. 3.4.

(a)  (b) 

Figure 3.4: Brass cell: (a) top view; (b) bottom view.

To accurately measure the interfacial temperature, a thermocouple is inserted into the tiny orifice at the interface height (Fig. 3.5). It is worth highlighting that the correlation between the temperature set on the rheometer, which corresponds to the temperature on top of the Peltier plate, and the temperature at the interface was previously established.

Figure 3.5: Detail of the orifice to thermocouple insertion.

The brass cell was made in two parts, as shown in Fig. 3.6, to facilitate cleaning, which is very important between tests, even more if the material tested varies. The geometry can be easily mounted by fitting the pieces together.

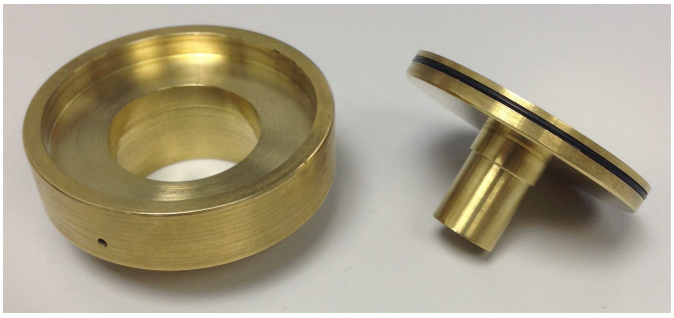

Figure 3.6: Two parts of the brass cell.

We also developed an insulation cap (Fig. 3.7) to minimize heat transfer from the surroundings and to hold the brass cell fixed and centered within the Peltier plate. It is made of plastic and fits perfectly in the DHR-3 Peltier plate. An orifice for the thermocouple was also made at the correspondent of the interface height of the insulation cap.

(a) 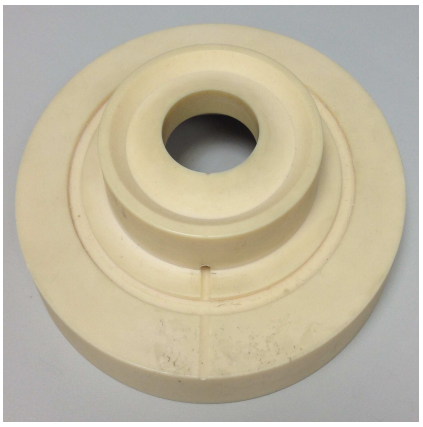 (b) 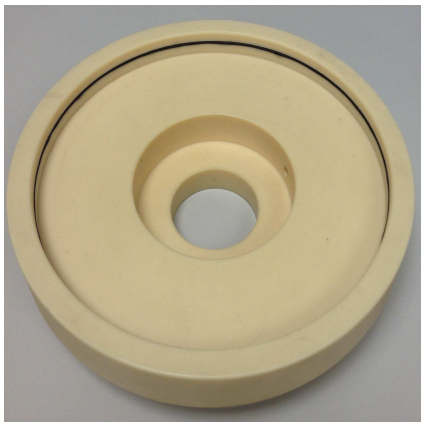

Figure 3.7: Insulation cap: (a) top view; (b) bottom view.

Furthermore, a cover for humidity control was seen to be necessary during the first test attempts (Fig. 3.8) mainly because of the temperature variation during experiments. It is made on plastic and also avoids sample contamination from outside dust.

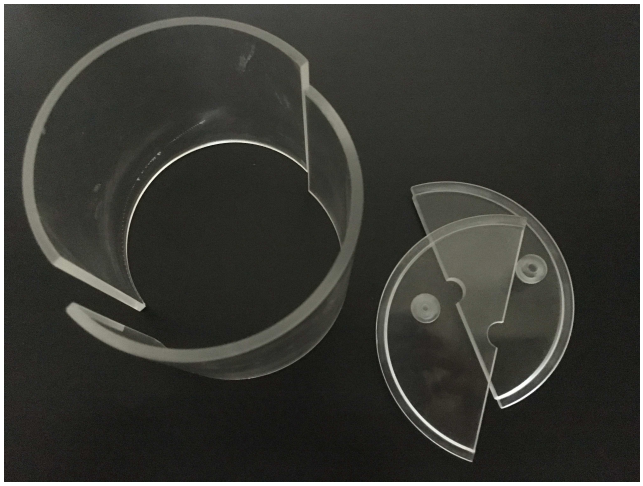

Figure 3.8: Isolation cover.

To enhance its performance, the cover is used with blue silica beads, shown in Fig. 3.9, that absorb condensed moisture. These beads adsorb water readily, being useful as a desiccant (drying agent). Once saturated with water, they can be regenerated by heating it to $\approx 120^{o}$C for 1 or 2 hours.

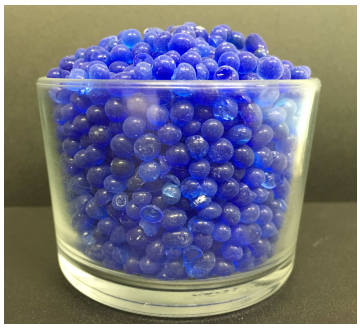

Figure 3.9: Silica beads for humidity control.

It is worth mentioning that the brass cell and its accessories were designed with the purpose to assess hydrate crystal growth at the interface between water and cyclopentane, but it can be used in different applications.

3.2 Setting up the experiment

For every run, the interfacial rheology testing platform is assembled. The brass cell is mounted and positioned at the center of the DHR-3 Peltier Plate, holden by the insulation cap. Some silica beads are laid in the insulation cap and one in the middle of the inner cylinder of the brass cell. It is important to replace the silica beads at the begging of each test because the spheres pop when exposed to enough water.

After that, $\approx$ 1.8 mL of water is cautiously loaded to the brass cell using a graduated pipette. Care is taken in order to avoid water from wetting the inner walls of the brass cell above the step mark. Then, the ring is placed at the surface. Finally, the cover for humidity control is installed.

Figure 3.10 illustrates the step by step procedure for setting up the apparatus and Figure 3.11 shows the rheometer equipped with the entire accessory, including the thermocouple.

A new water sample is used in each run.

Before starting the tests, a temperature conditioning step is applied to water: the interfacial temperature is stabilized at $T_{cond} = 20^{o}$C for 10 minutes. This pre-testing step guarantees that all experiments start at the same temperature.

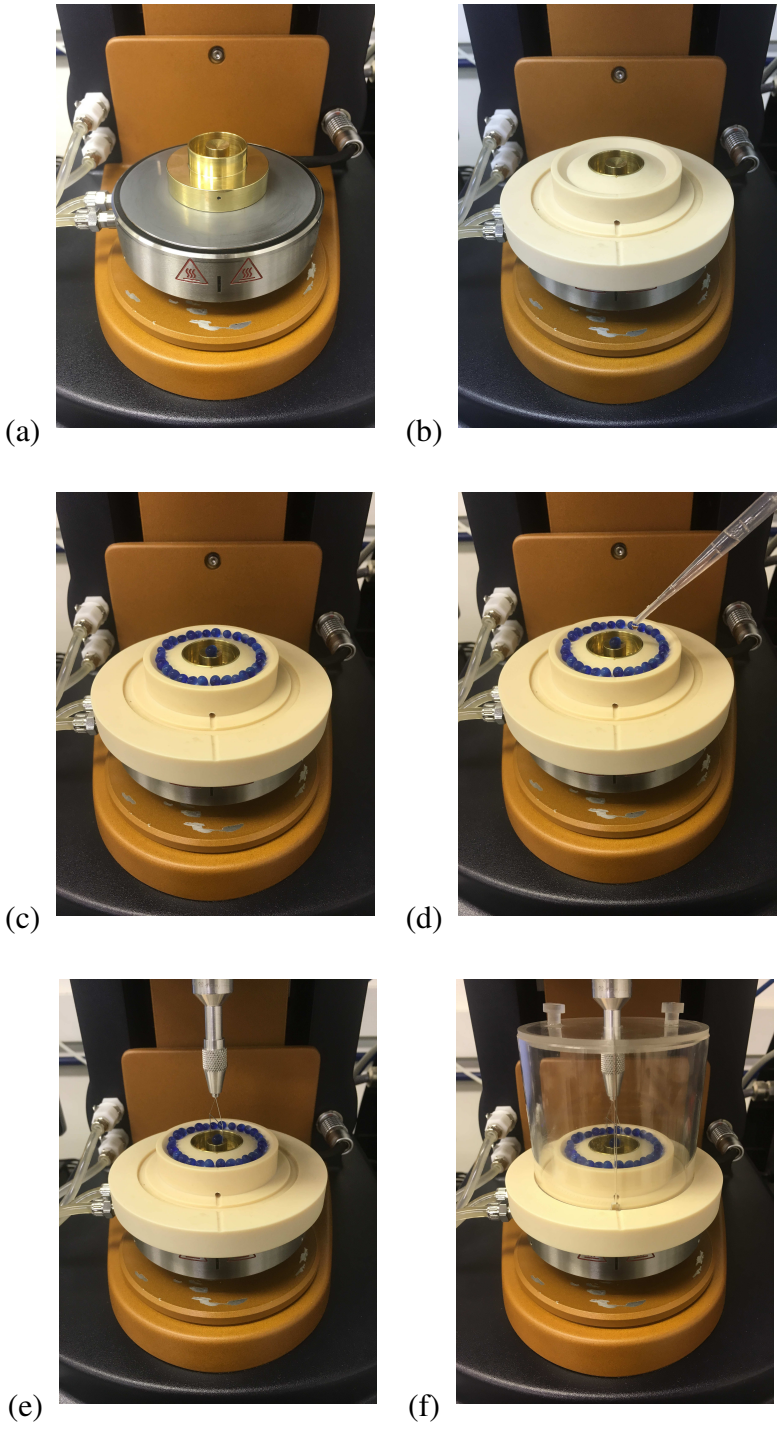

Figure 3.10: Steps for setting up the experiments.

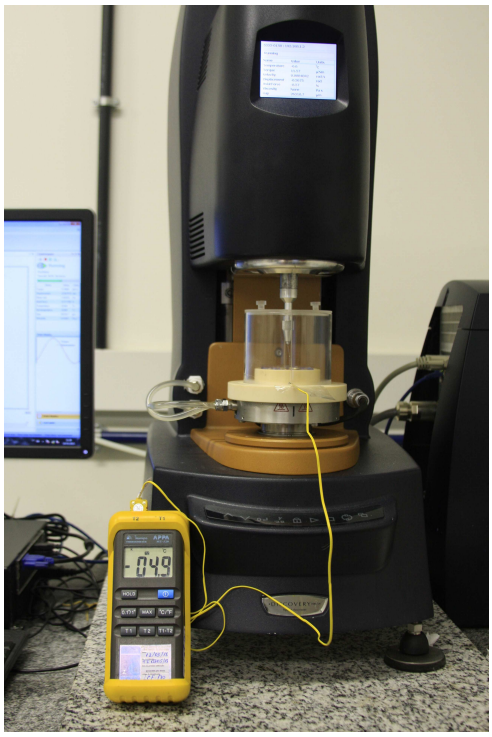

Figure 3.11: DHR-3 rheometer equipped with the entire accessory.

3.3 Rheometric experiments

A set of rheometric experiments was carried out to test the new geometry and characterize the kinetics of hydrate formation. After the conditioning step, time sweeps were performed in two stages in order to track down the behavior of the storage and loss modulus (G' and G'') of the water/cyclopentane interface and evaluate possible changes in it. If the interface is stable, no changes occur in the moduli. In each stage, a fixed frequency of 1 Hz and a constant strain amplitude of 0.05% are applied while the values of G' and G'' are recorded over time.

In the first stage, water is cooled down from $T_{cond} = 20^{o}$C to $T_i = -5^{o}$C at a rate of -2.5^{o}C/min. Then, the temperature is held at $T_i = -5^{o}$C for 10 minutes to assure that the entire sample solidifies, holding the ring.

In the second stage, cyclopentane (at room temperature) is added on top of ice at the same time that the temperature is increased to a final value (T_f) above the melting point of ice at a rate of 5.0^{o}C/min. Time starts to be counted from this moment. After that, the temperature is held at T_f for 1 hour and, if hydrate formation occurs, it is directly followed through measurement of the interfacial moduli. The final temperature was varied from 2^{o}C to 8^{o}C.

Figure 3.12 shows how the system is inside the cell during tests, after adding all components. The hydrate film is restricted to the interface between water and cyclopentane. None of these components is completely consumed.

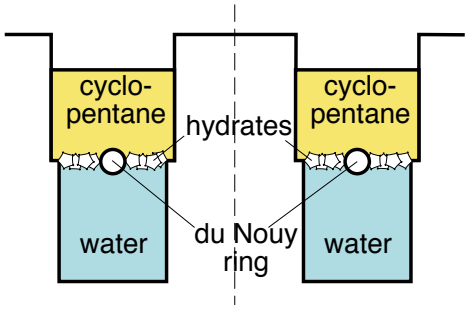

Figure 3.12: Illustration of how the system is inside the cell during tests.

The cooling and heating rates applied, namely -2.5^{o}C/min and 5.0^{o}C/min, were the maximum ones that the Peltier system used could achieve and maintain. These values were determined at previous test.

An overview of the experimental temperature profile is exhibited in Fig. 3.13.

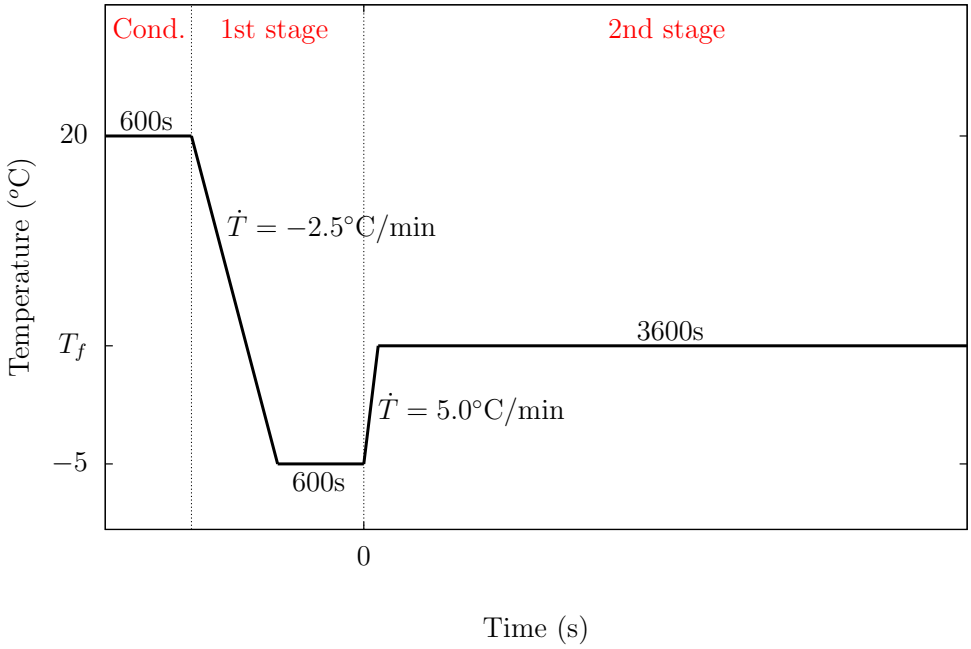

Figure 3.13: Summary of the experimental temperature profile during time sweeps.

For the cases in which hydrate formation was observed, steady state was achieved after a few minutes. Immediately after that, a strain sweep was carried out. It was run at the final temperature (T_f) so as to get information about hydrate mechanical properties and determine the linear viscoelastic region. This region is where G' and G'' are constant and parallel to each other. In these experiments, the strain is swept from 0.01% to 100% while the frequency is kept fixed at 1Hz.

3.4
Correction to account for the torsional strain of the du Nouy ring

In interfacial oscillatory tests, the rheometer output for the interfacial moduli G' and G'' does not account for an additional strain due to compliance of the du Nouy ring that arises from the long and slender rods holding it. Therefore, G' and G'' recorded must be corrected by equations 1 and 2 given below in order to obtain the proper interfacial moduli of the cyclopentane/water interface.

The actual interfacial storage modulus, G', and loss modulus, G'', are calculated from the effective shear modulus of the ring G_r, separately measured, and from the uncorrected storage and loss moduli of the assembly (G'_u and G''_u), supplied by the rheometer. More details on the correction are given in Appendix A.

$$G' = \frac{G_r G'_u (G_r - G'_u) - G''^2_u}{G'^2_u + G''^2_u + G_r(G_r - 2G'_u)} \tag{1}$$

$$G'' = \frac{G_r G''_u}{G_r - G'_u} + \frac{G''_u}{G_r - G'_u}\left(\frac{G_r G'_u (G_r - G'_u) - G''^2_u}{G'^2_u + G''^2_u + G_r(G_r - 2G'_u)}\right) \tag{2}$$

The results presented in the next chapter (Chap. 4) were corrected by these equations.

4
Results and Discussion

The results presented in this chapter are included in our recently published work “Growth Kinetics and Mechanics of Hydrate Films by Interfacial Rheology” [104].

4.1
Time sweep tests

A raw outcome of a time sweep experiment, including the two stages, is presented in Figure 4.1. It illustrates what can be seen as output during rheometric experiments. The conditioning step is not shown in this graphic, so time $t = 0\,\mathrm{s}$ corresponds to the beginning of the first stage. The filled symbols represent the storage modulus (G'_u) while the empty symbols indicate the loss modulus (G''_u). This is the only result presented in this chapter without the correction of the moduli formulated in the previous chapter (Chap. 3) being applied. As detailed in Appendix A, this correction will not drastically change the interfacial modulus behavior but will generate some adjustments.

As explained before, during the first stage, after being cooled to $T_f = -5^{\mathrm{o}}\mathrm{C}$, the temperature is kept constant for 600 s. A steep increase in the storage modulus (G'_u) is observed at $t \approx 700\,\mathrm{s}$, while the loss modulus (G''_u) remains lower. This means that the elastic behavior of the sample overlaps the viscous, indicating the appearance of the first ice seeds. A few seconds later, the storage modulus achieves its highest plateau which signalizes the complete solidification of the water sample. Then, at $\approx 1200\,\mathrm{s}$, the cyclopentane is added on top of the ice block and the temperature is heated to the final value, in this case $T_f = 3^{\mathrm{o}}\mathrm{C}$. The G' plateau lasts for a few more seconds and then drops abruptly when the ice block melts completely. After that, the storage modulus starts increasing again, this time at a lower rate and at a temperature above the melting point of ice. This indicates the beginning of hydrate formation. A few seconds later, the increasing rate diminishes. Less than 10 minutes after the appearance of the first hydrate structures, G' reaches again a higher plateau, meaning that a stable hydrate film was formed at the interface between water and cyclopentane.

All the stages described above, namely ice formation, ice melting and hydrate

formation, could be checked visually during the experiments.

The plateau indicating ice formation is higher than the one indicating hydrate formation because a solid ice block appears during the first stage while only a layer of hydrate arises at the interface during the second stage.

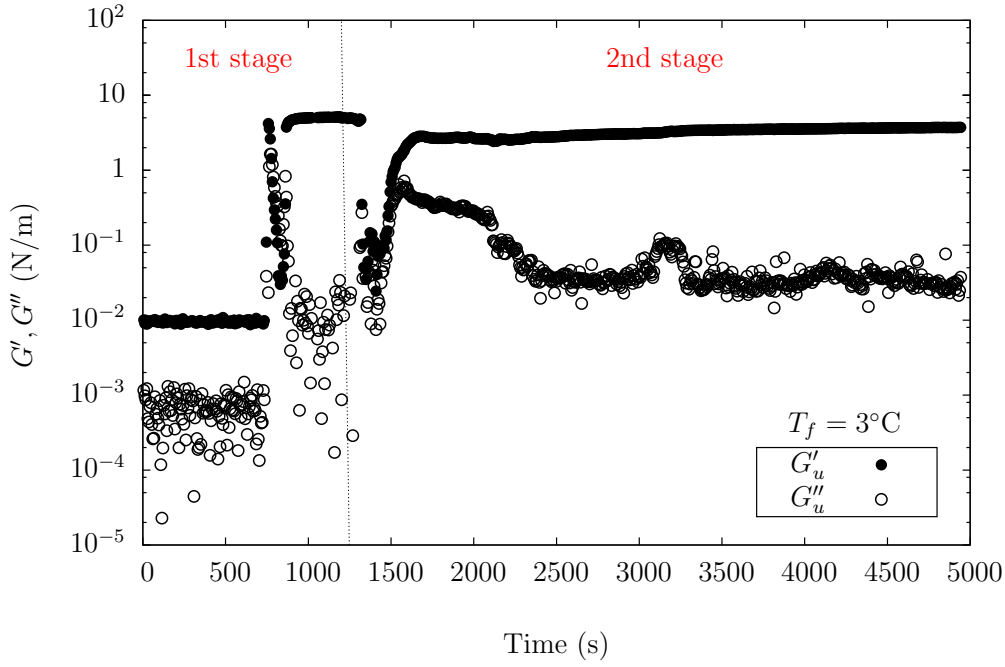

Figure 4.1: Raw complete time sweep outcome.

Since the interest here is to track down the kinetics of the hydrate crystals, we will focus only on the second stage hereinafter. The only objective of the first stage is to convert water into ice in order to enable the hydrate formation on the second stage, as it will be addressed later. The graphic outcome of that stage is the same for all the experiments. Therefore, it will be omitted.

The outcome of the second stage of time sweep experiments is shown in Figures 4.2 - 4.8 for a set of final temperatures (T_f = 2°C, 3°C, 4°C, 5°C, 6°C, 7°C and 8°C). In these graphics, time t = 0 s corresponds to the cyclopentane addition (onset of second stage, see previous Section 3.3). The filled symbols indicate the storage interfacial modulus (G') while the empty symbols indicate the loss interfacial modulus (G''). Three pairs of curves are plotted for each final temperature: each one corresponds to a different run carried out with a fresh sample at the same conditions. All the moduli were corrected by equations 1 and 2 presented before.

Figures 4.2 - 4.6 display the kinetics of hydrate film formation as the interfacial moduli grow with time. The results reveal that these films are viscoelastic once they possess both interfacial storage and loss moduli. However, their elastic nature supersedes the viscous response by an order of magnitude.

In all cases, an almost instantaneous drop (close to $t = 0\,\text{s}$) of the interfacial moduli is observed. It indicates the melting of the ice block formed during the previous stage.

After that, the moduli growth starts within a few seconds following addition of the cyclopentane ($t = 0\,\text{s}$). Some minutes later, the increasing rate diminishes. Then, the moduli take time scales on the order of tens of minutes to reach an asymptotic limit. It can be observed that this limit occurs earlier at higher temperatures, meaning that the growth time diminishes with temperature. The referred limit expresses the structure of a stable hydrate film, that isolates the water and cyclopentane subphases (which are immiscible). Consequently, hydrate formation stops and the film does not grow anymore. During the experiments, the existence of the hydrate film was visually confirmed.

A distinct overshoot in the moduli is observed at $t \approx 500\,\text{s}$ in all tests. It is even more significant in the ones run at lower temperatures. It presumably reveals a restructuring of the hydrate network at the beginning: it takes some time for the hydrates to form a stable film, indicated by the plateau. Before that, not all the nuclei formed achieve the critical size required for continued growth due to the metastable state, explained in Section 2.2.2.

It is worth noting that, once the hydrate film is formed, each of the interfacial moduli G' and G'' can be approximated as the product of the corresponding bulk hydrate moduli (G'_{bulk} and G''_{bulk}) with the thickness of the hydrate film. During the experiments managed in this work, visualization at the interface height and access to the hydrate film are impossible. Consequently, hydrate film thickness was not directly measured. Thus the interfacial moduli G' and G'' should be regarded as effective interfacial moduli.

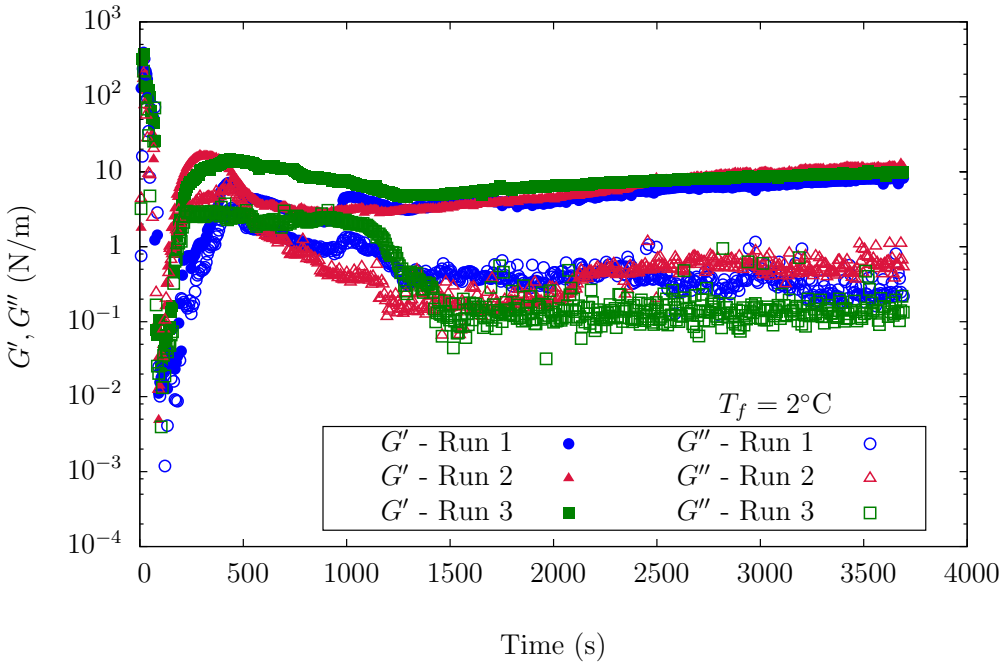

Figure 4.2: Time sweep outcome for water/cyclopentane interface at $T_f = 2^{\circ}$C. The initial time $t = 0$ s corresponds to the moment when the cyclopentane is added and the temperature is increased. Hydrate is formed.

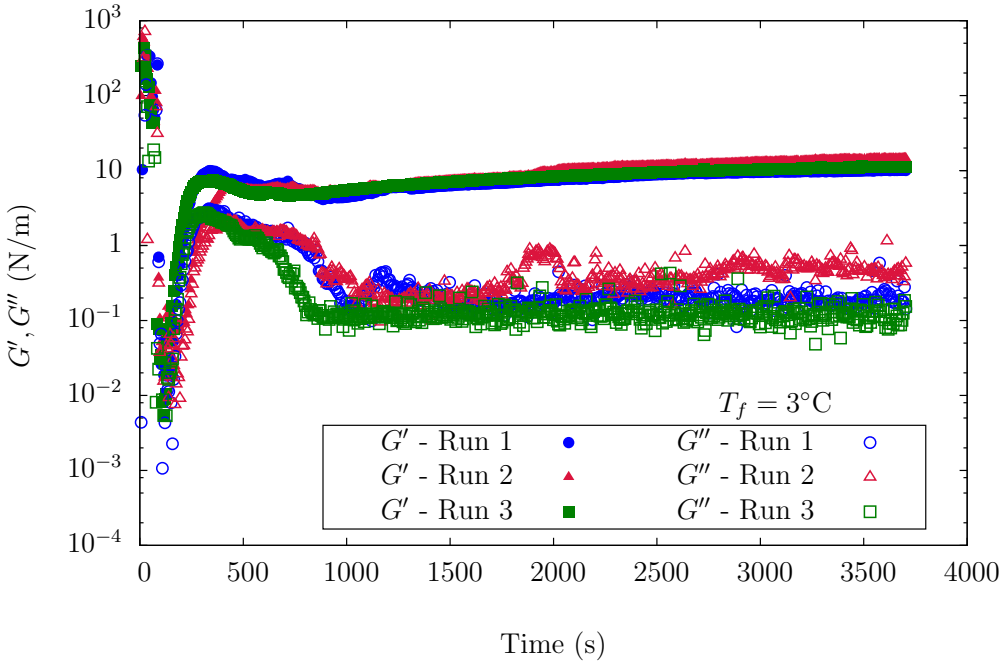

Figure 4.3: Time sweep outcome for water/cyclopentane interface at $T_f = 3^{\circ}$C. The initial time $t = 0$ s corresponds to the moment when the cyclopentane is added and the temperature is increased. Hydrate is formed.

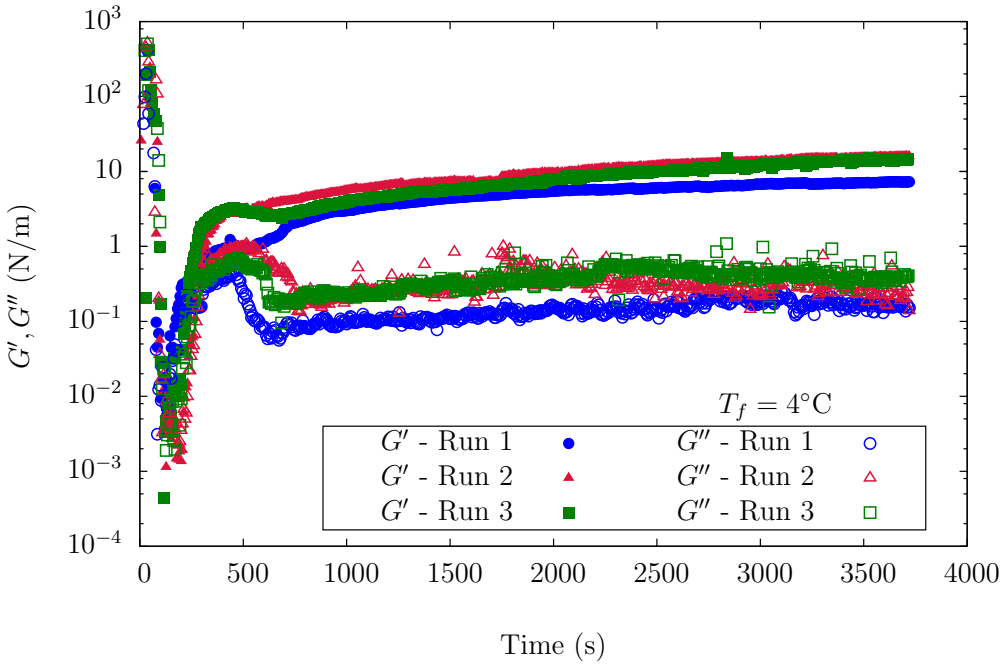

Figure 4.4: Time sweep outcome for water/cyclopentane interface at $T_f = 4^{\circ}$C. The initial time $t = 0$ s corresponds to the moment when the cyclopentane is added and the temperature is increased. Hydrate is formed.

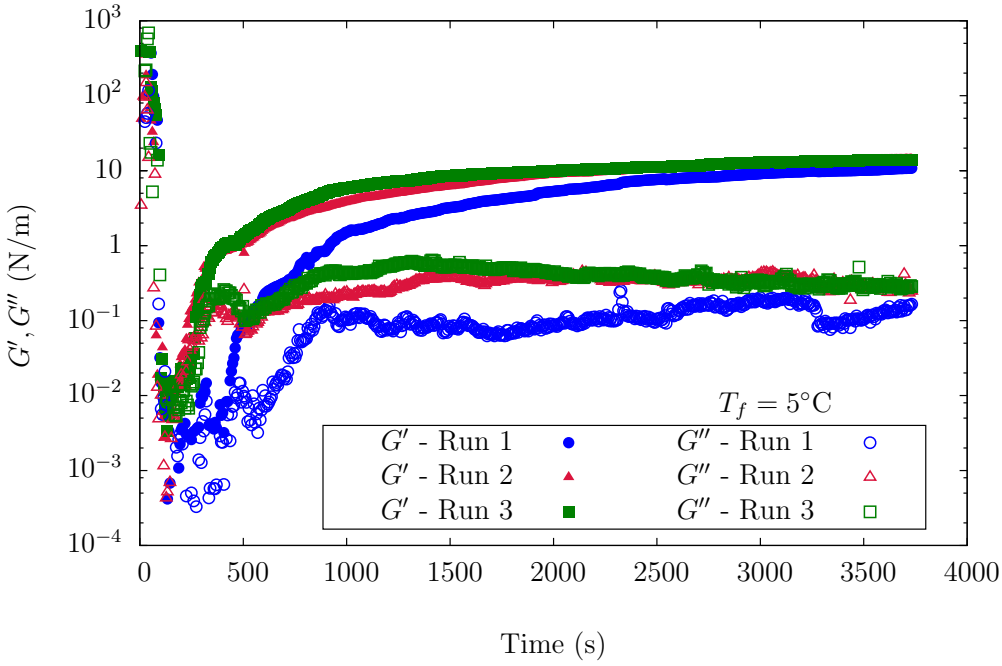

Figure 4.5: Time sweep outcome for water/cyclopentane interface at $T_f = 5^{\circ}$C. The initial time $t = 0$ s corresponds to the moment when the cyclopentane is added and the temperature is increased. Hydrate is formed.

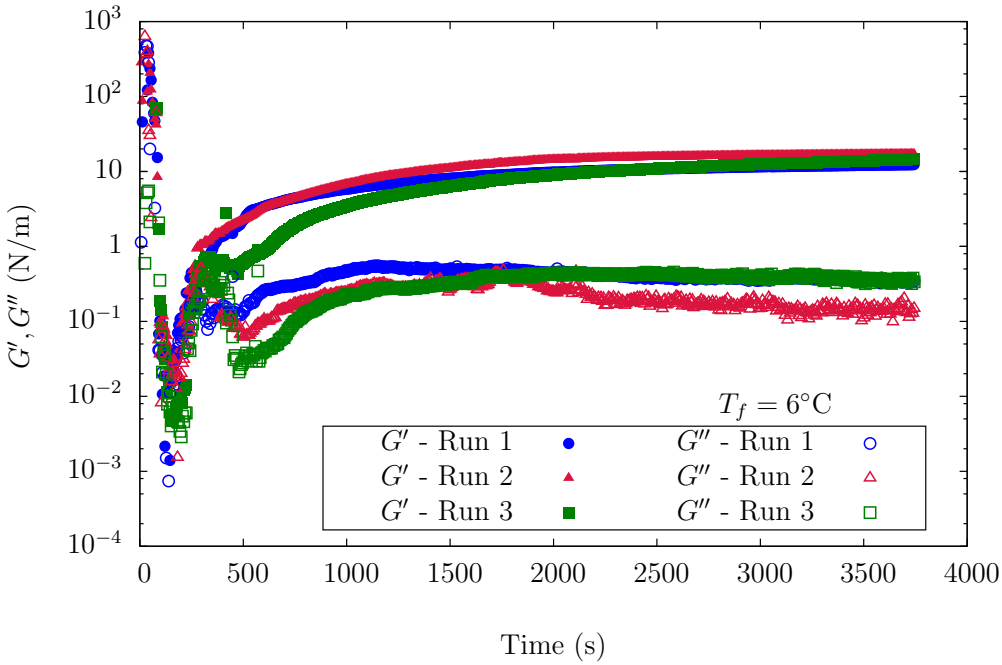

Figure 4.6: Time sweep outcome for water/cyclopentane interface at $T_f = 6^{o}$C. The initial time $t = 0$ s corresponds to the moment when the cyclopentane is added and the temperature is increased. Hydrate is formed.

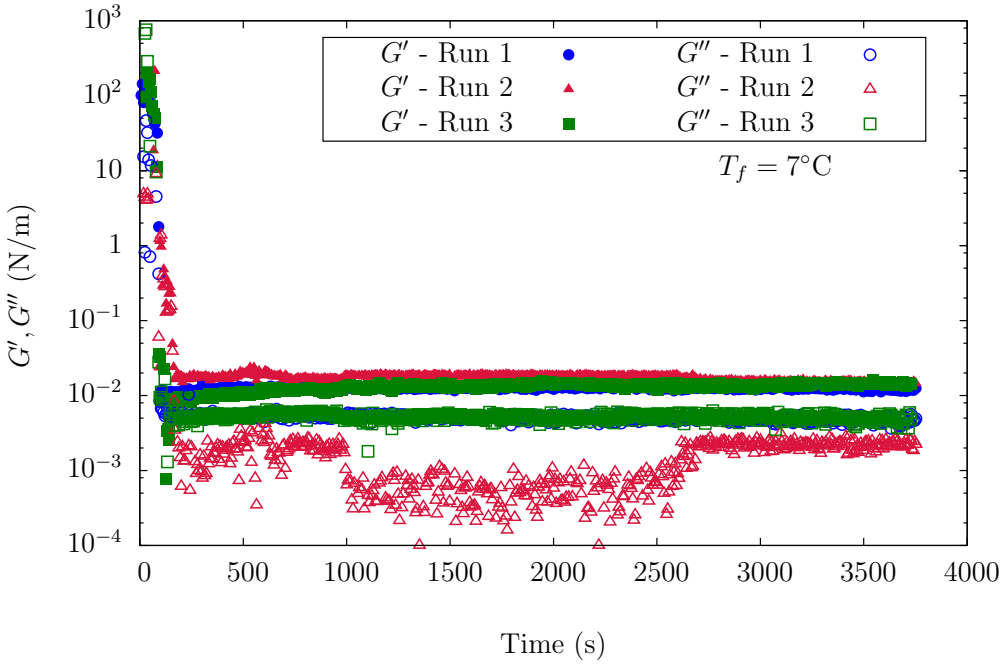

Figure 4.7: Time sweep outcome for water/cyclopentane interface at $T_f = 7^{o}$C. The initial time $t = 0$ s corresponds to the moment when the cyclopentane is added and the temperature is increased. Hydrate is not formed.

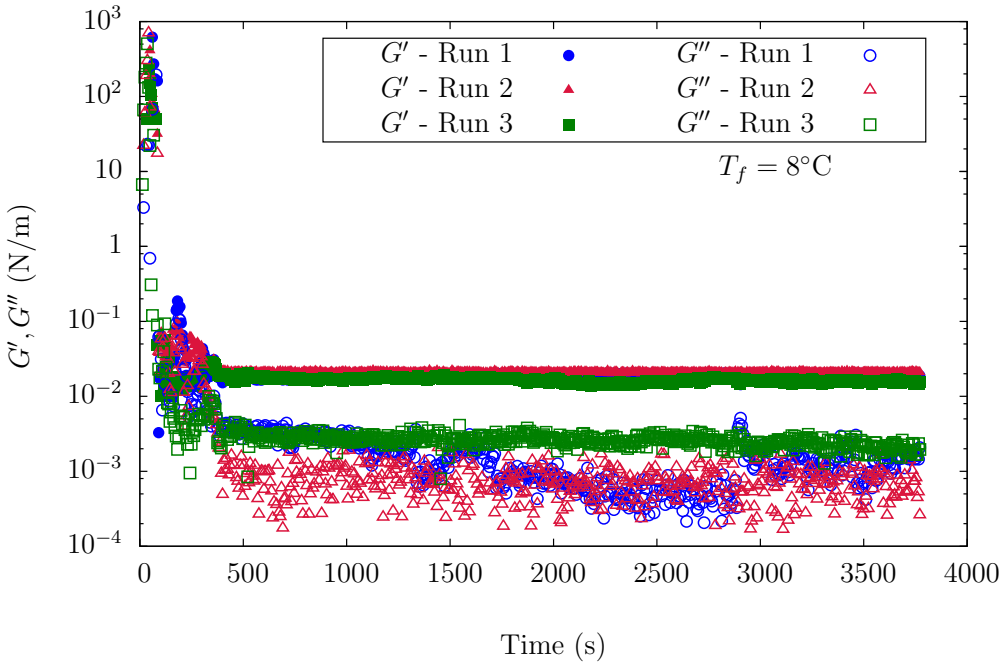

Figure 4.8: Time sweep outcome for water/cyclopentane interface at $T_f = 8^{o}$C. The initial time $t = 0$ s corresponds to the moment when the cyclopentane is added and the temperature is increased. Hydrate is not formed.

In Figures 4.7 and 4.8, at $T_f = 7^{o}$C and $T_f = 8^{o}$C respectively, the system behavior is completely different from the previously analyzed. No hydrate formation is observed as the interfacial moduli remain very small. This indicates that within 1 hour (time duration of the second stage), the maximum temperature at atmospheric pressure in which cyclopentane hydrates form is below these temperatures. Furthermore, the results also show that this maximum temperature is above $T_f = 6^{o}$C, since hydrates were formed at this final temperature.

This temperature should not be confused with the dissociation temperature. As stated before, there is a fundamental difference between the formation point and the dissociation point due to hydrate metastability (see Fig. 2.4). Considering the reported dissolution temperature of cyclopentane hydrates at atmospheric pressure, 7.7^{o}C [43, 92, 97], it is plausible to conclude that probably at $T_f = 7^{o}$C the cyclopentane/water interface is at the metastable zone while at $T_f = 8^{o}$C, it is to the right of the dissolution line, as illustrated in Figure 4.9. Thereby, hydrates could not be detected in any of these temperatures. It is possible that hydrate formation would occur at $T_f = 7^{o}$C if a longer test were performed.

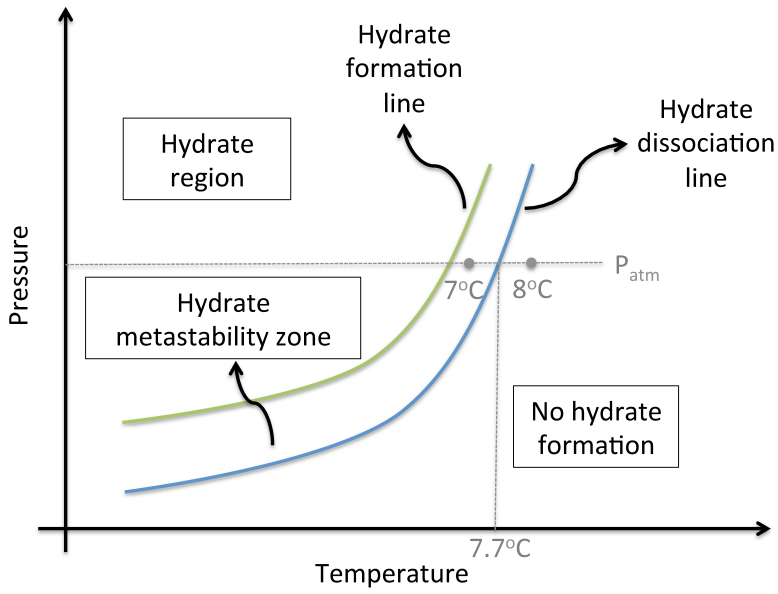

Figure 4.9: Cyclopentane hydrate phase diagram scheme: probably at 7°C, the system is inside the metastability zone and at 8°C, it is inside the hydrate free region.

It is important highlighting that, in the tests in which hydrates are not formed, the rheometer signal (torque) is too low. Thus, these tests are only qualitatively used as indicators of hydrate absence. Further physical analysis should not be done regarding the values of the storage and loss interfacial moduli.

4.1.1 Effect of T_f on the interfacial storage modulus

Once the time evolution of the interfacial moduli has been acquired for chosen values of T_f, several characteristics of the kinetic responses can be retrieved. Figure 4.10 illustrates the progression in the steady state values of the interfacial storage modulus G' for the different final temperatures. The error bars indicate the scatter. It is worth highlighting that, as explained in Section 2.2.2, hydrate formation is a stochastic process and the deviations presented are based on three experiments for each temperature only.

The data suggest that the storage modulus increases as T_f increases, revealing that the hydrate films formed at temperatures closer to the dissociation temperature (which is $T_f = 7.7^{\circ}$C) are more structured than the ones formed at lower temperatures. The maximum deviation is 5 N/m for $T_f = 4^{\circ}$C.

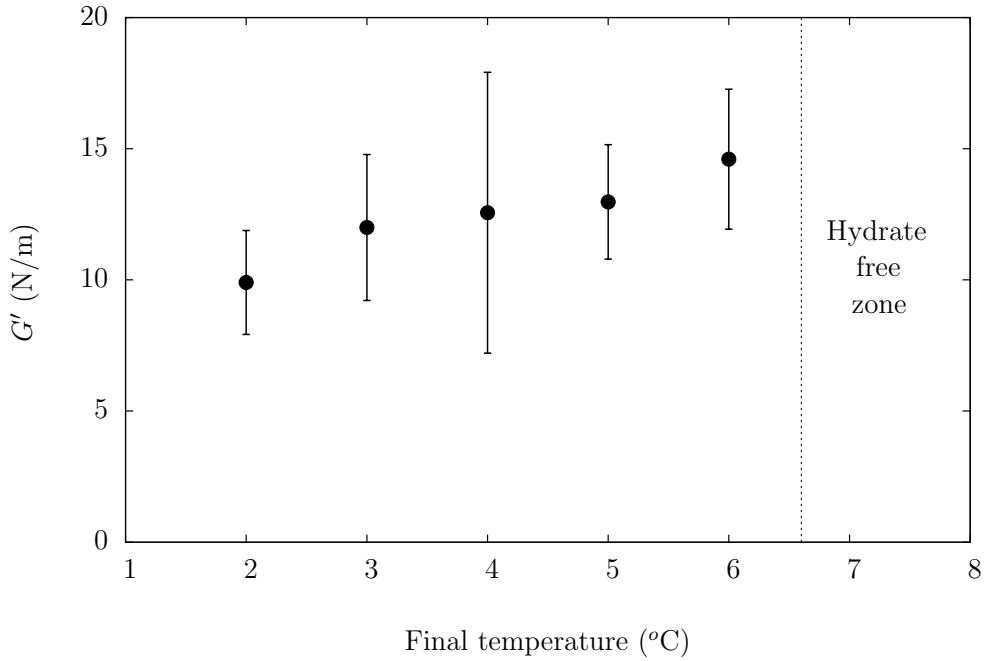

Figure 4.10: Interfacial elastic modulus (obtained from the steady state plateau of the time sweep tests) as a function of the final temperature: G' increases as T_f is increased. Deviations are based on three experiments for each temperature.

4.1.2 Effect of T_f on the critical time

The critical time, t_c, is defined as the time for the inception of the abrupt modulus rise measured following the cyclopentane addition, at each final temperature. Figure 4.11 shows a comparison between the critical times measured at each one of them. Again, the error bars indicate the scatter and the deviations presented are based on three run experiments for each temperature.

The time for the onset of hydrate formation seems to increase as T_f increases, probably due to the low driving forces. It means that the higher the final temperature, the longer it takes for the first hydrate structures to appear. This is in agreement with previous works that showed a trend between the degree of subcooling (defined as the difference between the dissociation temperature and the set temperature) and the critical time as higher subcoolings lead to shorter critical times [105, 106].

The maximum deviation on critical time is 15 s for $T_f = 4^{\circ}$C.

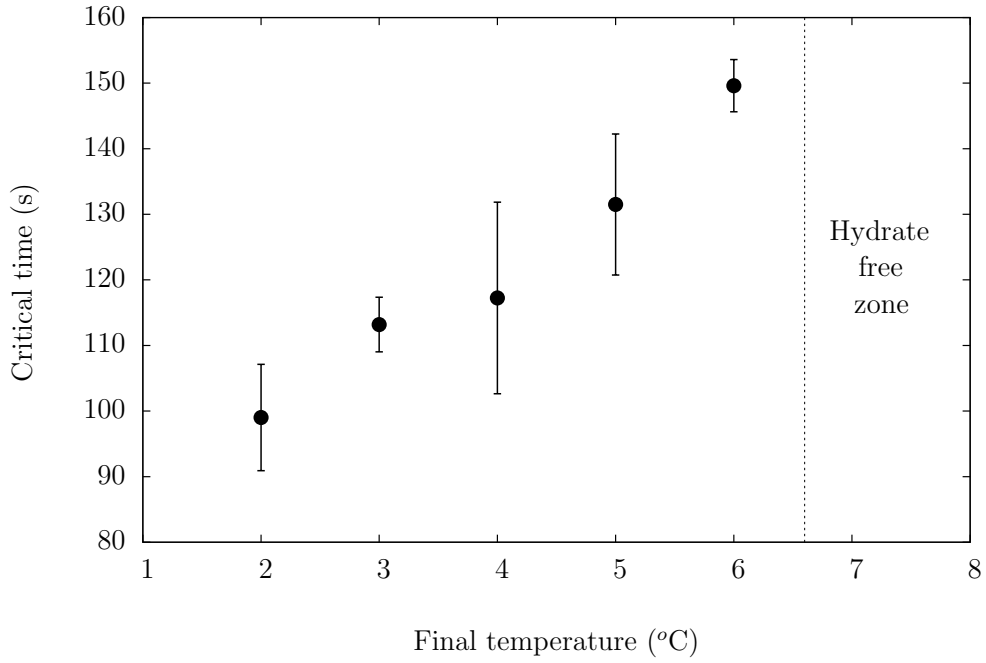

Figure 4.11: The critical time (t_c) - the time for the onset of hydrate formation during time sweep tests - as a function of the final temperature: t_c increases as T_f is increased. Deviations are based on three experiments for each temperature.

4.1.3 Ice seeding

The interfacial rheology testing platform offers the flexibility to probe the mechanism of hydrate formation by systematically altering the protocol described above where cyclopentane was directly contacted with ice before rapidly transitioning to a higher temperature, T_f. Figure 4.12 shows the interfacial moduli where layered samples of cyclopentane resting on water were directly cooled to a temperature $T = T_f = 5^{\circ}$C. This procedure differs from the described in Chapter 3 by the absence of the first stage in which ice is formed. Unlike Figures 4.2 - 4.6, where the kinetics of hydrate formation is clearly seen, there is an absence of hydrate formation displayed in Figure 4.12. This finding demonstrates that hydrate formation within 1 hour (second stage of time sweep experiments running time) requires that the cyclopentane layer first be exposed and caged by crystalline water molecules.

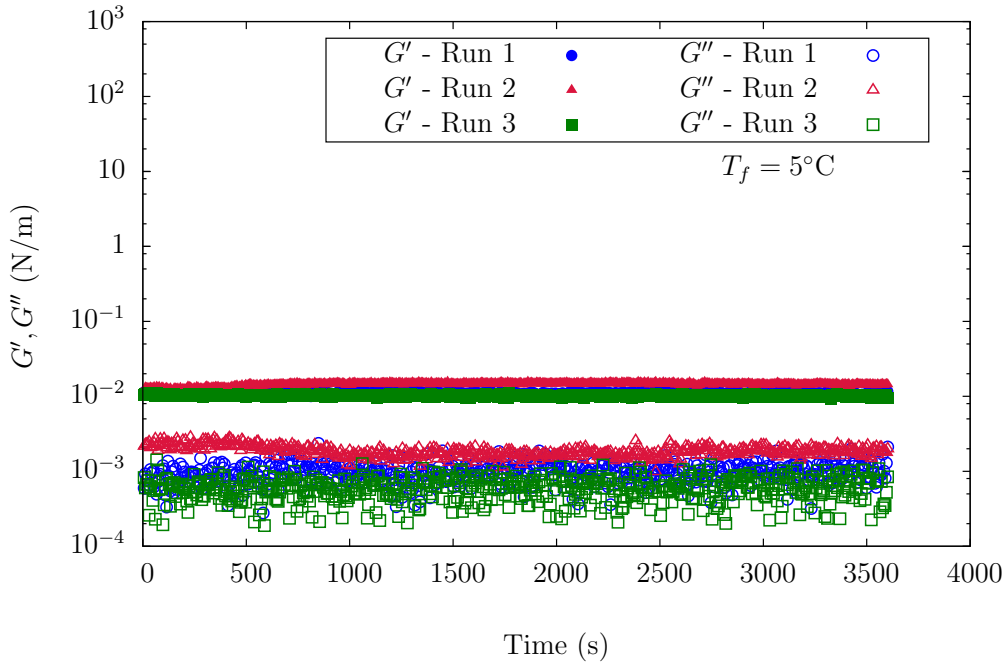

Figure 4.12: Time sweep at $T_f = 5^{o}$C during the entire test: no hydrate is formed without first exposing the cyclopentane to ice.

To further explore the initial condition required for hydrate formation, the experiment resulting in Figure 4.13 was carried out. In this case, ice was allowed to form, as evidenced by the large moduli at time $t = 0$ s. Then, the temperature was increased to $T_f = 5^{o}$C (without CP addition at this moment) and kept constant for 10 minutes, time enough for the small block of ice to melt completely. Cyclopentane was added at $t = 600$ s only, after all the ice structures being destroyed, and again no hydrate was formed. This reaffirms that ice formation is indispensable in our test protocol.

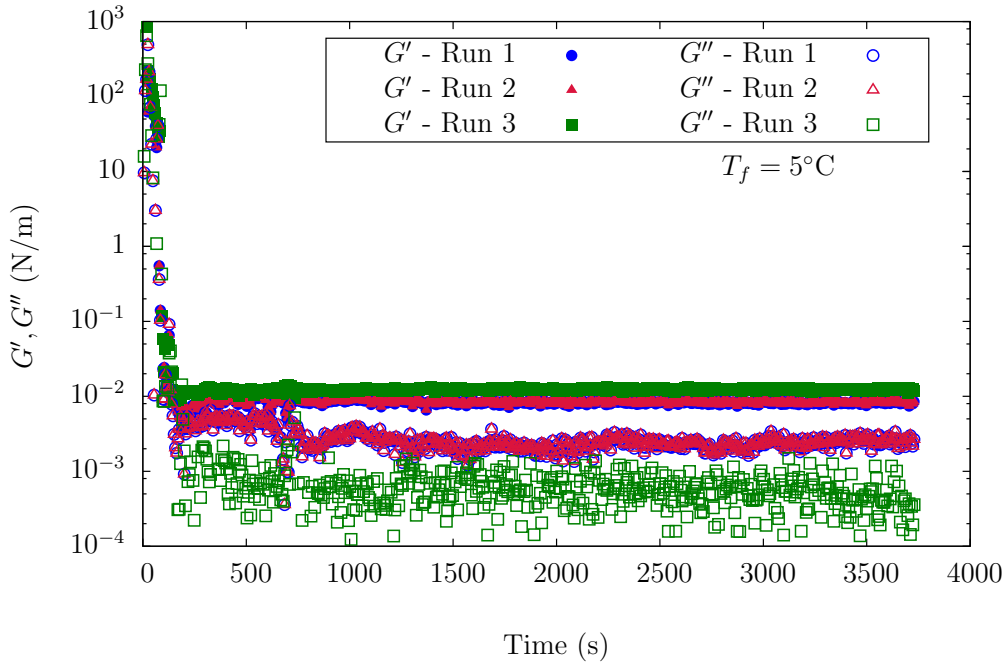

Figure 4.13: Time sweep carried out with cyclopentane being added at $t = 600$ s, after complete ice melting: no hydrate is formed.

As discussed in Chapter 2 (Sec. 2.2.2), the existence of a "memory effect" is controversial. The two last outcomes, analyzed among the ones previously presented (Figures 4.2 - 4.6), obtained with ice presence, appear to support its existence. The attendance of ice molecular structures when cyclopentane is added seems to, at least, accelerate the formation of hydrates (once it occurs within our test duration), given that hydrate formation was clearly detected in all ice-laden tests below the dissolution temperature (Fig. 4.2 - 4.6) but in none without ice seeds (Fig. 4.12 and 4.13). Indeed, as demonstrated in other works [38, 45], ice can trigger hydrate nucleation because of its hydrogen-bonded crystal structure that is similar to the hydrate crystal structure.

On the other hand, the subcooling effect should also be considered. It is possible that hydrate is formed in the cases in which CP is added on top of ice below the dissolution temperature (Fig. 4.12 and 4.13), but not when it is added on top of water (Fig. 4.12 and 4.13), because the subcooling is higher in those cases. Therefore, the nucleation would happen in a lower temperature (before the system reaches T_f), consequently generating growth even after the increase in temperature. The temperature at which the cyclopentane is added into the cell could be determining in this case.

4.2
Strain sweep tests

Following the conclusion of each time sweep experiment that resulted in a hydrate film appearance (i.e. when $T_f \leq 6^{\circ}$C), a strain sweep test was performed at the same final temperature, T_f. One result for each one of the final temperatures is illustrated in Figures 4.14 - 4.18. The interfacial storage modulus (G') is represented by the filled symbols while the interfacial loss modulus (G'') is represented by the empty symbols. From these tests, it is possible to identify the range of linear viscoelasticity, where the moduli are strain independent and the yield strain beyond which the interfacial moduli start decreasing. All outcomes are similar and demonstrate that the hydrate films are fragile and break down when sheared at low values of yield strain (in the neighborhood of 0.6%).

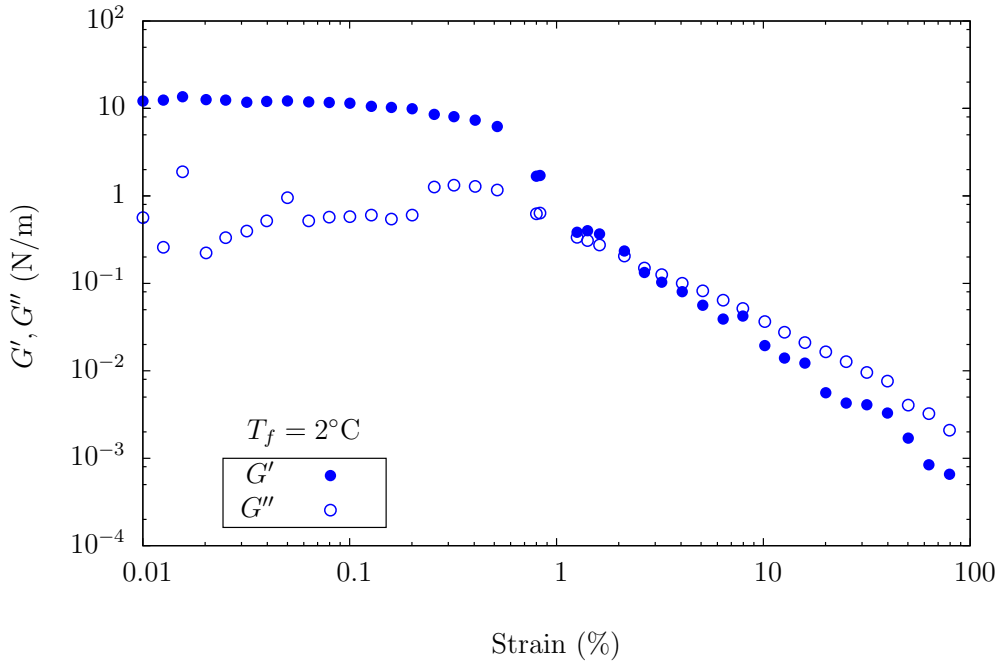

Figure 4.14: Strain sweep outcome performed after hydrate formation at $T_f = 2^{\circ}$C.

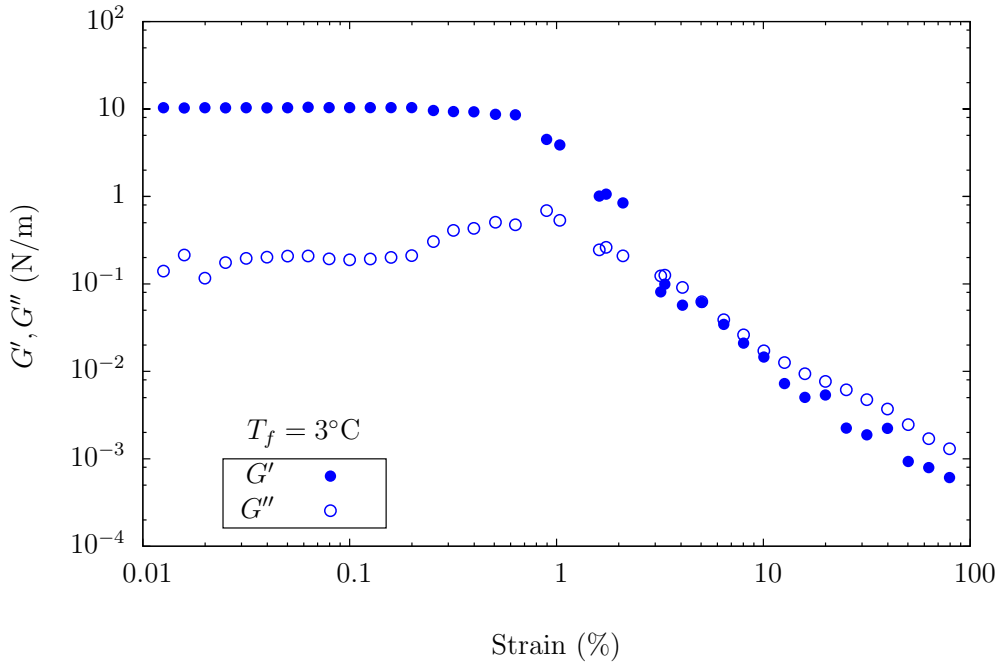

Figure 4.15: Strain sweep outcome performed after hydrate formation at T_f = 3°C.

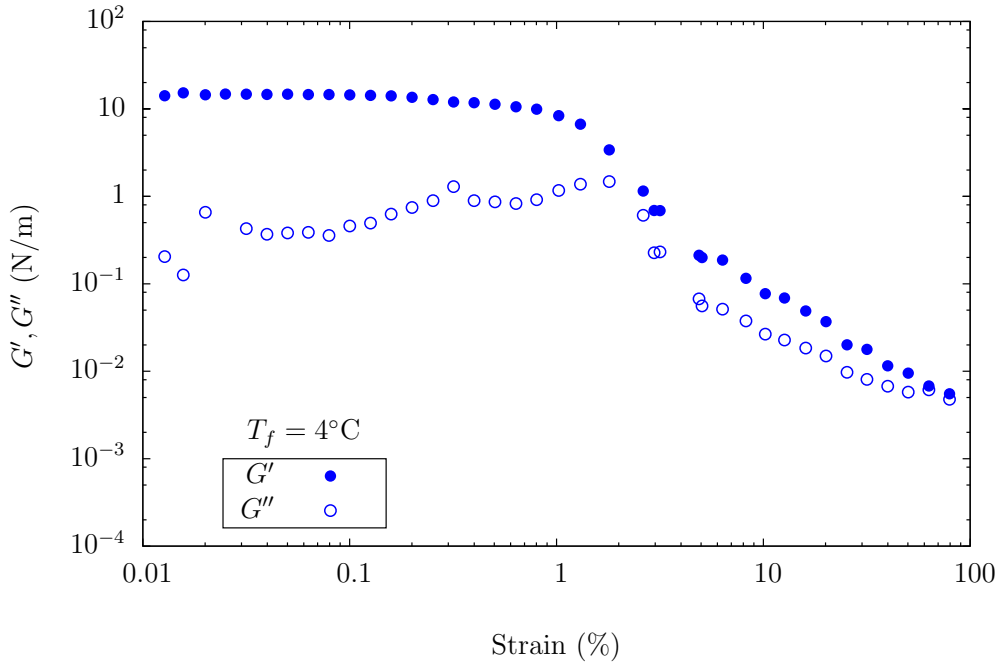

Figure 4.16: Strain sweep outcome performed after hydrate formation at T_f = 4°C.

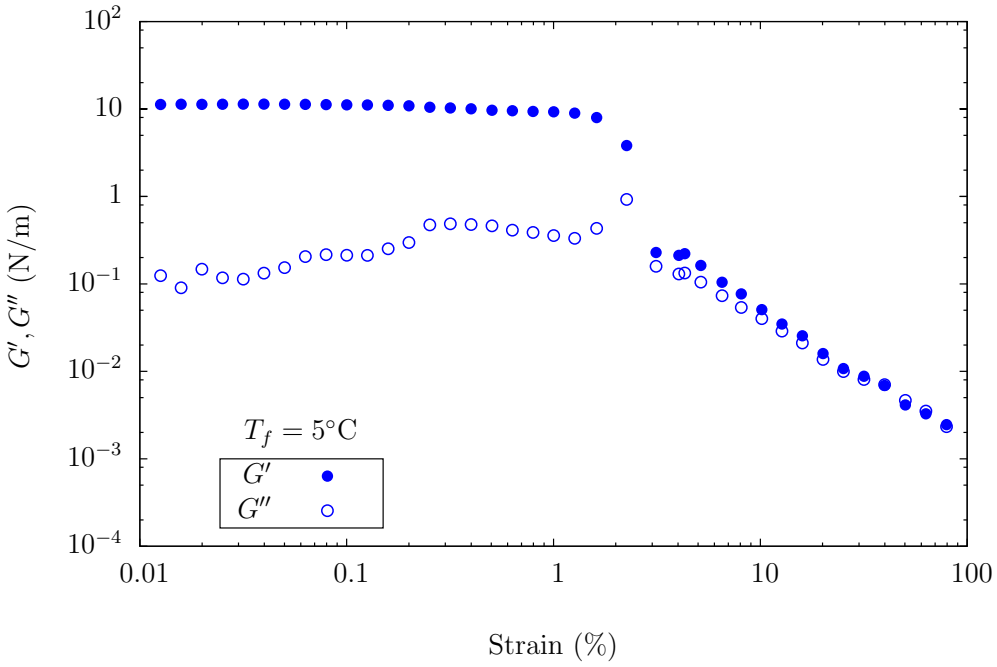

Figure 4.17: Strain sweep outcome performed after hydrate formation at T_f = 5^{o}C.

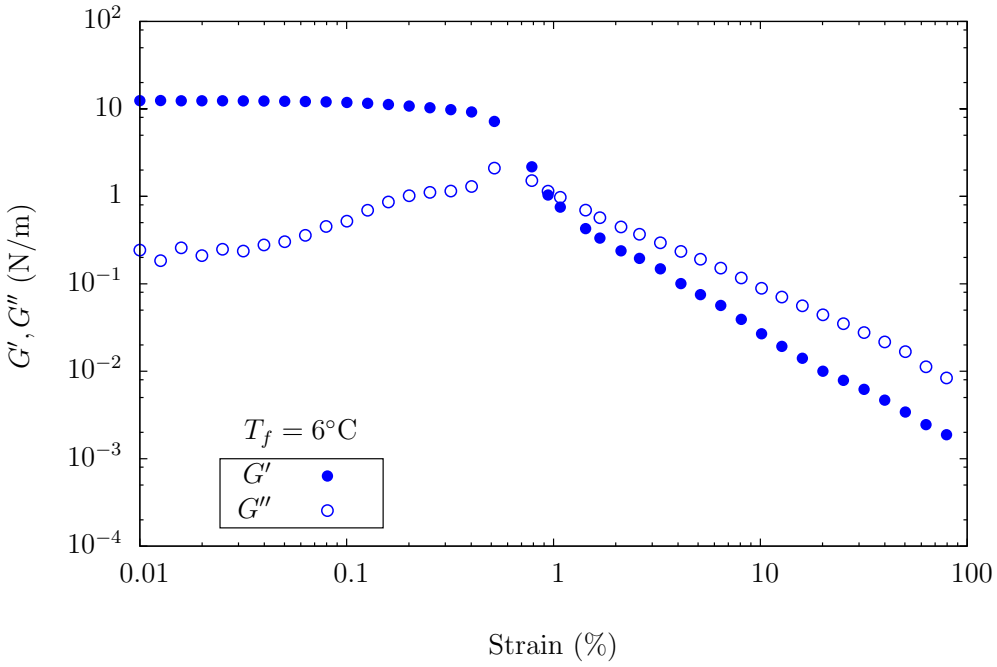

Figure 4.18: Strain sweep outcome performed after hydrate formation at T_f = 6^{o}C.

4.2.1
Effect of T_f on the yield strain

Figure 4.19 shows the tendency of the interfacial yield strain as a function of the final temperature. Each point corresponds to the average of the three tests run at each final temperature. The yield strain increases as the final temperature is increased, meaning that the hydrate films formed at temperatures closer to the dissociation temperature are capable of sustaining larger elastic strains.

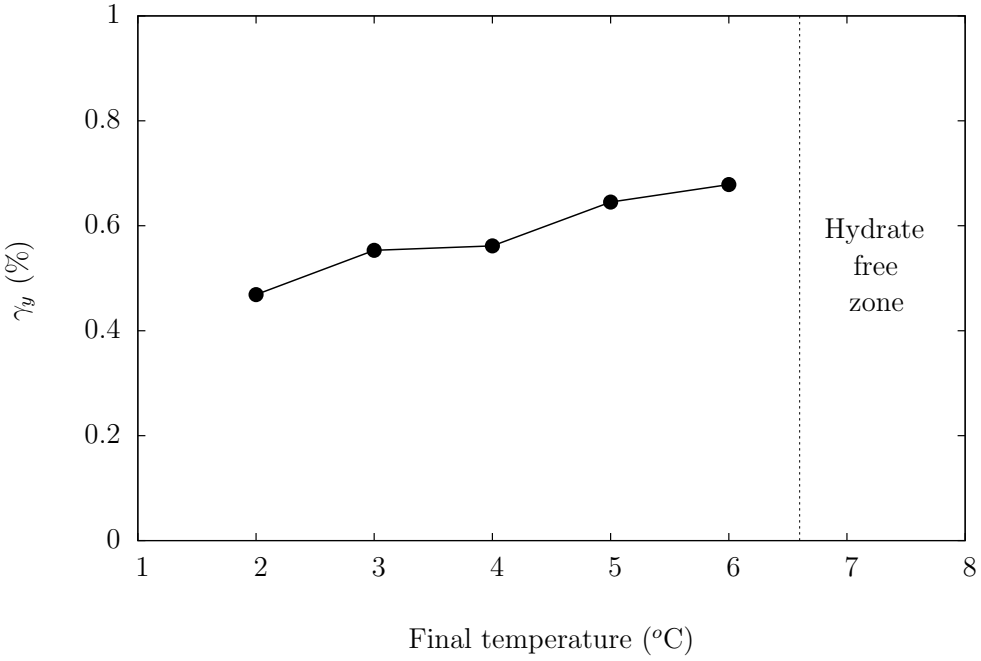

Figure 4.19: Interfacial yield strain as a function of the final temperature: γ_y increases as T_f is increased.

5
Concluding Remarks

As discussed before, both interfacial rheology and hydrates are wide fields yet being boosted. Driven by the lack of studies on how the interface between a hydrocarbon and water behaves during nucleation and growth of hydrates, this work ended up reporting advances in both of the cited fields. In the first, by developing a modified double wall ring cell for interfacial moduli measurements which proved to be effective in allowing a temperature variation. Its usage is not limited to the study of hydrate films - as was done here. The brass cell can also be used with the du Nouy ring to measure properties of other systems, such as the interface between water and oil, that is relevant, for example, in emulsification processes.

In the second, by experimentally investigating the growth kinetics of cyclopentane hydrate films. It was verified that measuring interfacial moduli offers a very sensitive indication of hydrate growth, what is not accessible with observational approaches and without the complicated influences of emulsion mechanisms associated with previous rheological studies. Consequently, this approach offers the promise to determine the kinetics of hydrate growth under various conditions as well as the mechanical strength of the resulting structures. Thus, the findings made during this research can be of useful help for further development on the numerous hydrate applications.

A protocol for hydrate forming tests using the new interfacial geometry was developed. It consists of two time sweep stages - one for ice formation and onother for hydrate formation - followed by a strain sweep test. Cyclopentane is only added to the system at the beginning of the second stage of the time sweep and the interfacial modulus behavior is monitored during the entire experiment.

It was possible to establish a qualitative idea of the hydrate films behavior. Time sweeps at interfacial final temperatures from 2^{o}C to 8^{o}C following the initial cyclopentane/ice contact were presented. Two behavior types were observed. For $T_f = 2^{o}$C, 3^{o}C, 4^{o}C, 5^{o}C and 6^{o}C, the interfacial storage modulus started increasing almost immediately after cyclopentane addition, reaching an asymptotic limit a few minutes later. This signalizes the formation of a hydrate film at the interface that was visually confirmed.

For $T_f = 7^{o}$C and 8^{o}C, the outcome was completely different. The storage

modulus did not change after CP addition. Thereby, the maximum temperature at atmospheric pressure at which cyclopentane hydrate arises was identified to be between 6^{o}C and 7^{o}C. Because the dissociation temperature of CP hydrates is known to be 7.7^{o}C, we concluded that, at 7^{o}C, the system is at the hydrate metastability zone, meaning that the critical size for continued growth was not achieved by the microscopic hydrate crystals during the experiments.

It was shown that the presence of ice at the time of cyclopentane addition is necessary for hydrate formation within the time duration of our tests. Two hypotheses can be made. The first is that it happens mostly because of the hydrogen bonds promoted by ice, which points out to the existence of the controversial "memory effect". This justifies the existence of the first stage on the established protocol - temperature is kept below the melting point of ice to solidify water in order to trigger further hydrate formation. If enough amount of heat is provided to the system during a prolonged period of time, the "memory effect" is extinguished (see Figure 4.13). The second hypothesis is that the subcooling significantly affects hydrate formation. When CP is added on top of ice, the subcooling is higher and the first hydrate crystals appear faster. Once the nucleation happens, the growth process is a consequence (even if the temperature increases a few more degrees) as long as the final temperature is below the dissociation temperature. This also justifies the existence of the first stage on the established protocol. In this case, the temperature at which the cyclopentane is added into the cell could be crucial.

Strain sweep experiments were also carried out at the final temperatures in which hydrate film formation had been detected (from 2^{o}C to 6^{o}C). In these tests, the hydrate interfacial moduli are measured as functions of the applied strain. The results showed that the hydrate films formed during the previous time sweep experiments are fragile.

Because a set of final temperatures was assessed, some comparisons between the results obtained at each one of them could be made. Data suggested the following trends as T_f is increased: (i) the critical time for hydrate formation t_c; (ii) the interfacial elastic modulus G' and (iii) the yield strain γ_y all increase. It means that the closer the final temperature is to the dissociation temperature, the longer it takes for the first hydrate structures to appear, but it also means that, after full development, the hydrate films formed at those temperatures will be more structured and able to sustain larger elastic strains.

An important interfacial modulus correction to account for the torsional strain of the du Nouy ring was introduced in Section 3.4. The actual interfacial storage and loss moduli are calculated from the effective shear modulus of the ring G_r, separately measured, and from the uncorrected storage and loss moduli of the assembly (G'_u and G''_u), supplied by the rheometer. The equations are deducted and

better explained in Appendix A. A comparison between raw and corrected data is shown and highlights the importance of the correction of the moduli for future interfacial experiments with ring geometries.

5.1 Suggestions for future research works

The creation of the new brass cell with temperature control enables a wide range of different interfacial measurements. Thus, future steps may include, for example, the evaluation of the heating rate effect on the critical time and final G' plateau. Some past studies showed that thermodynamic conditions are a primary factor controlling the formation and dissociation of hydrates and it seems that the melting rate of ice directly affects the nucleation of hydrates.

Besides that, investigation of the effects of nanoparticles, surfactants, anti-agglomerants or alcohols on hydrate crystal growth can also be carried out. The same protocol used in the present work could be applied, but adding dispersed particles in one of the sub-phases.

A deeper examination into the "memory effect" is also required. More experiments could be run using both hydrate and ice seeding and the effect of subcooling should be investigated. It would be of great value to cool the cyclopentane to the final temperature before adding it to the test cell instead of adding it at room temperature.

Bibliography

[1] P. Englezos. Clathrate hydrates. *Ind. Eng. Chem. Res.*, 32:1251–1274, 1993.

[2] TA Instruments. *AR-G2 User Guide*.

[3] A. Sum. Gas hydrates in flow assurance workshop. Universidade Tecnológica Federal do Paraná - Curitiba, 2015.

[4] D. Sloan. Introductory overview: Hydrate knowledge development. *American Mineralogist*, 89:1155–1161, 2004.

[5] C. Koh, E. Sloan, A. Sum, and D. Wu. Fundamentals and applications of gas hydrates. *Annu. Rev. Chem. Biomol. Eng.*, 2:237–257, 2011.

[6] I. Chatti, A. Delahaye, L. Fournaison, and J. Petitet. Benefits and drawbacks of clathrate hydrates: a review of their areas of interest. *Energy Conversion and Management*, 46:1333–1343, 2005.

[7] D. Martinez. *Transporte de gás natural sob a forma de hidratos gasosos*. PhD thesis, Universidade Federal do Rio de Janeiro, Escola de Química, 2009.

[8] G. Zylyftari. *Hydrate Forming Emulsion: A Rheological, Thermodynamic and Morphological Study*. PhD thesis, The City College of New York, 2014.

[9] E. Sloan. A changing hydrate paradigm - from apprehension to avoidance to risk management. *Fluid Phase Equilibria*, 228-229:67–74, 2005.

[10] TA Instruments. *DHR-3 User Guide*.

[11] L. Mondy, C. Brooks, A. Grillet, H. Moffat, T. Koehler, M. Yaklin, M. Reichert, L. Walker, R. Cote, and J. Castañeda. Surface rheology and interface stability. Technical report, Sandia National Laboratories, 2010.

[12] H. Sun, L. Zhang, Z. Li, L. Zhang, L. Luo, and S. Zhao. Interfacial dilational rheology related to enhance oil recovery. *Soft Matter*, 7(17):7601–7611, 2011.

[13] M. Bos and T. Vliet. Interfacial rheological properties of adsorbed protein layers and surfactants: a review. *Advances in Colloid and Interface Science*, 91:437–471, 2001.

[14] B. Murray. Rheological properties of protein films. *Current Opinion in Colloid & Interface Science*, 16:27–35, 2011.

[15] J. Pelipenko, J. Kristl, S. Baumgartner, and P. Kocbek. Interfacial rheology: An overview of measuring techniques and its role in dispersions and electrospinning. *Acta Pharmaceutica*, 62(2):123–140, 2012.

[16] R. Miller and L. Liggieri, editors. *Progress in Colloid and Interface Science - Interfacial Rheology*, volume 1. Koninklijke Brill NV, 2009.

[17] S. Vandebril, A. Franck, G. Fuller, P. Moldenaers, and J. Vermant. A double wall-ring geometry for interfacial shear rheometry. *Rheologica Acta*, 49(2):131–144, 2010.

[18] S. Reynart, C. Brooks, P. Moldenaers, J. Vermant, and G. Fuller. Analysis of the magnetic rod interfacial stress rheometer. *Journal of Rheology*, 52(1):261–285, 2008.

[19] G. Fuller. Interfacial Rheology Webinar (TA Instruments).

[20] G. Fuller, F. Aloyse, and J. Vermant. System and method for interfacial rheometry. *US Patent 20090056423*, 2009.

[21] W. Wang, K. Li, P. Wang, S. Hao, and J. Gong. Effect of interfacial dilational rheology on the breakage of dispersed droplets in a dilute oil–water emulsion. *Colloids and Surfaces A: Physicochemical and Enginnering Aspects*, 441:43–50, 2014.

[22] K. Zhang and O. Ni. Effect of PIBSA-based surfactants on the interfacial interaction, rheology, and stability of highly concentrated water-in-oil emulsion. *Journal of Dispersion Science and Technology*, 36(4):556–562, 2015.

[23] L. Rosenfeld and G. Fuller. Consequences of interfacial viscoelasticity on thin film stability. *Langmuir*, 28(40):14238–14244, 2012.

[24] D. Harbottle, Q. Chen, K. Moorthy, L. Wang, S. Xu, Q. Liu, J. Sjoblom, and Z. Xu. Problematic stabilizing films in petroleum emulsions: Shear rheological response of viscoelastic asphaltene films and the effect on drop coalescence. *Langmuir*, 30(23):6730–6738, 2014.

[25] M. Reichert, N. Alvarez, C. Brooks, A. Grillet, L. Mondy, S. Anna, and L. Walker. The importance of experimental design on measurement of dynamic interfacial tension and interfacial rheology in diffusion-limited surfactant systems. *Colloids and Surfaces A: Physicochemical and Enginnering Aspects*, 467:135–142, 2015.

[26] G. Fuller and J. Vermant. Complex fluid-fluid interfaces: Rheology and structure. *The Annual Review of Chemical and Biomolecular Engineering*, 3:519–43, 2012.

[27] H. McConnell. Structures and transitions in lipid monolayers at the air-water interface. *Annual Review of Physical Chemistry*, 42:171–195, 1991.

[28] D. Sloan, C. Koh, A. Sum, N. McMullen, G. Shoup, A. Ballard, and T. Palermo. *Natural Gas Hydrates in Flow Assurance*. Gulf Professional Publishing by Elsevier Inc., 2011.

[29] G Aspenes. *The influence of pipeline wettability and crude oil composition on deposition of gas hydrates during petroleum production*. PhD thesis, University of Bergen, 2009.

[30] D. Sloan and C. Koh. *Clathrate Hydrates of Natural Gases*. Taylor and Francis, Boca Raton, FL., 2008.

[31] Bahman Tohidi. Applied gas hydrates. Hydrafact Ltd. & Centre for Gas Hydrate Research - Heriot-Watt University, 2016.

[32] J. Peixinho, P. Karanjkar, J. Lee, and J. Morris. Rheology of hydrate forming emulsions. *Langmuir*, 26(14):11699–11704, 2010.

[33] E. Sloan. Clathrate hydrates: The other common solid water phase. *Industrial and Engineering Chemistry Research*, 39:3123–3129, 2000.

[34] Z. Huo, E. Freer, M. Lamar, B. Sannigrahiand D. Knaussand, and E.Sloan. Hydrate plug prevention by anti-agglomeration. *Chem. Eng. Sci.*, 56:4979–4991, 2001.

[35] Y. Fujioka, K. Takeuchi, Y. Shindo, and H Komiyama. Shrinkage of liquid CO_2 droplets in water. *Intl. J. Energy Res.*, pages 765–769, 1994.

[36] D. Kashchiev and A. Firoozabadi. Nucleation of gas hydrates. *Journal of Crystal Growth*, 243(3):476–489, 2002.

[37] C. Taylor. *Adhesion Force between Hydrate Particles and Macroscopic Investigation of Hydrate Film Growth at the Hydrocarbon/Water Interface*. PhD thesis, Colorado School of Mines, Golden, CO, 2006.

[38] G. Zylyftari, A. Ahuja, and J. Morris. Nucleation of cyclopentane hydrate by ice studied by morphology and rheology. *Chemical Engineering Science*, 116:497–507, 2014.

[39] P. Bishnoi and V Natrajan. Formation and decomposition of gas hydrates. *Fluid Phase Equilib.*, 117:168–177, 1996.

[40] J. Parent. *Investigations into Nucleation Behavior of the Clathrate Hydrates of Natural Gases*. PhD thesis, University of Calgary, Alberta, 1993.

[41] V. Bansal. *Kinetic Study of Clathrate Hydrates*. PhD thesis, Colorado School of Mines, 1994.

[42] P. Wilson, D. Lester, and A. Haymet. Heterogeneous nucleation of clathrates from supercooled tetrahydrofuran (THF)/water mixtures, and the effect of an added catalyst. *Chem. Eng. Sci.*, 60:2937–2941, 2005.

[43] E. Dirdal, C. Arulanantham, H. Sefidroodi, and M Kelland. Can cyclopentane hydrate formation be used to rank the performance of kinetic hydrate inhibitors? *Chemical Engineering Science*, (177-184), 2012.

[44] Y. Mori. Formation of CO_2 hydrate on the surface of liquid CO_2 droplets in water - some comments on a previous paper. *Energy conversion and management*, 39(5):369–373, 1998.

[45] S. Takeya, A. Hondoh, and T. Uchida. Freezing-memory effect of water on nucleation of CO_2 hydrate crystals. *J. Phys. Chem. B*, 104(17):4164–4168, 2000.

[46] C. Moon, P. Taylor, and P. Rodger. Molecular dynamics study of gas hydrate formation. *J. Am. Chem. Soc.*, 125(16):4706–4707, 2003.

[47] R. Radhakrishnan and B. Trout. A new approach for studying nucleation phenomena using molecular simulations: Application to CO_2 hydrate clathrates. *J. Chem. Phys.*, 117:1786–1796, 2002.

[48] B. Sowa and N. Maeda. Statistical study of the memory effect in model natural gas hydrate systems. *J. Phys. Chem. A*, 119(44):10784–10790, 2015.

[49] R. Ohmura, M. Ogawa, K Yasuoka, and Y. Mori. Statistical study of clathrate-hydrate nucleation in a water/hydrochlorofluorocarbon system: Search for the nature of the "memory effect". *J. Phys. Chem. B*, 107(22):5289–5293, 2003.

[50] C. Duchateau, J. Peytavy, P. Glénat, T. Pou, M.Hidalgo, and C Dicharry. Laboratory evaluation of kinetic hydrate inhibitors: A procedure for enhancing the repeatability of test results. *Energy Fuels*, 23(2):962–966, 2009.

[51] A. Vysniauskas and P. Bishnoi. A kinetic-study of methane hydrate formation. *Chem. Eng. Sci.*, 38(7):1061–1072, 1983.

[52] H. Sefidroodi, E. Abrahamsen, and M. Kelland. Investigation into the strength and source of the memory effect for cyclopentane hydrate. *Chem. Eng. Sci.*, 87:133–140, 2013.

[53] D. Kashchiev and A. Firoozabadi. Driving force for crystallization of gas hydrates. *Journal of Crystal Growth*, 241:220–230, 2002.

[54] P. Wilson and A. Haymet. Hydrate formation and re-formation in nucleating THF/water mixtures show no evidence to support a "memory" effect. *Chemical Engineering Journal*, 161:146–150, 2010.

[55] P. Buchanan, A. Soper, H. Thompson, R. Westacott, J. Creek G. Hobson, and C Koh. Search for memory effects in methane hydrate: Structure of water before hydrate formation and after hydrate decomposition. *The Journal of Chemical Physics*, 123:164507–1–164507–7, 2005.

[56] D. Bond and N. Russell. Effect of antifreeze agents on the formation of hydrogen sulphide hydrate. *Transactions of the AIME*, 179:192–198, 1949.

[57] E. Hammerschmidt. Preventing and removing gas hydrates formations in natural gas pipelines. *Oil & Gas Journal*, 37(52):66–72, 1939.

[58] U. Karaaslan and M. Parlaktuna. Surfactants as hydrate promoters? *Energy & Fuels*, 14:1103–1107, 2000.

[59] D. York and A. Firoozabadi. Comparing effectiveness of rhamnolipid biosurfactant with a quaternary ammonium salt surfactant for hydrate anti-agglomeration. *J. Phys. Chem. B*, 112:845–851, 2008.

[60] X. Li, L. Megadi, and A. Firoozabadi. Anti-agglomeration in cyclopentane hydrates from bio- and co-surfactants. *Energy & Fuels*, 24:4937–4943, 2010.

[61] J. Slattery and R. Robinson. Effects of induced convection upon the rate of crystallization. *Chemical Engineering Science*, 51(9):1357–1363, 1996.

[62] K. Kvenvolden. Gas hydrates - geological perspective and global change. *Reviews of Geophysics*, 31(2):173–187, 1993.

[63] Y. Makogon. Natural gas hydrates - a promising source of energy. *Journal of Natural Gas Science and Engineering*, 2(1):49–59, 2010.

[64] A. Milkov. Global estimates of hydrate-bound gas in marine sediments: how much is really out there? *Earth-Science Reviews*, 66(3-4):183–197, 2004.

[65] J. Bohannon. Weighing the climate risks of an untapped fossil fuel. *Science*, 319:1753, 2008.

[66] S. Kang and H. Lee. Recovery of CO_2 from flue gas using gas hydrate. *Journal of Crystal Growth*, 34:4397–4400, 2000.

[67] H. Srivastava ans G. Sastry. Viability of clathrate hydrates as CO_2 capturing agents: A theoretical study. *The Journal of Physical Chemistry A*, 115:7633–7637, 2011.

[68] J. Gudmundsson, M. Mork, and O. Graff. Hydrate non-pipeline technology. In *4th International Conference on Gas Hydrates*, pages 997–1102, 2002.

[69] W. Mao, H. Mao, A. Goncharov, V. Struzhkin, Q. Guo, J. Hu, J. Shu, R. Hemley, M. Somayazulu, and Y. Zhao. Hydrogen clusters in clathrate hydrate. *Science*, 297:2247–2249, 2002.

[70] Y. Dyadin, E. Larionov, A. Manakov, F. Zhurko, E. Aladko, T. Mikina, and V. Komarov. Clathrate hydrates of hydrogen and neon. *Mendeleev Communications*, 9:209–210, 1999.

[71] R. Kumar, H. Wu, and P. Englezos. Incipient hydrate phase equilibrium for gas mixtures containing hydrogen, carbon dioxide and propane. *Fluid Phase Equilibria*, 244:167–171, 2006.

[72] J. Zhang and J. Lee. Equilibrium of hydrogen + cyclopentane and carbon dioxide + cyclopentane binary hydrates. *J. Chem. Eng. Data*, 54:659–661, 2009.

[73] M. van Denderen, E. Ineke, and M. Golombok. CO_2 removal from contaminated natural gas mixtures by hydrate formation. *Ind. Eng. Chem. Res.*, 48:5802–5807, 2009.

[74] D. Pereira. *Detecção de subprodutos da desinfecção com cloro em água dessalinizada*. Dissertação para mestrado em química, Faculdade de Ciências da Universidade do POrto, 2007.

[75] J. Sangwai, R. Patel, P. Mekala, D. Mech, and M. Busch. Desalination of seawater using gas hydrate technology – current status and future direction. In *Proceedings of HYDRO 2013 International*, pages 434–440, 2013.

[76] K. Park, S. Hong, J. Lee, K. Kang, Y. Lee, M. Ha, and J. D. Lee. A new apparatus for seawater desalination by gas hydrate process and removal characteristics of dissolved minerals (Na^+, Mg^{2+}, Ca^{2+}, K^+, B^{3+}). *Desalination*, 274:91–96, 2011.

[77] G. von Medeazza. Water desalination as a long-term sustainable solution to alleviate global freshwater scarcity? a north-south approach. *Desalination*, 169:287–301, 2004.

[78] A. Delahaye, L. Fournaison, S. Jerbi, and N. Mayoufi. Rheological properties of CO_2 hydrate slurry flow in the presence of additives. *Ind. Eng. Chem. Res.*, 50:8344–8353, 2011.

[79] T. Ogawa, T. Ito, K. Watanabe, K.i Tahara, R. Hiraoka, J. Ochiai, R. Ohmura, and Y. Mori. Development of a novel hydrate-based refrigeration system: A preliminary overview. *Applied Thermal Engineering*, 26:2157–2167, 2006.

[80] P. Zhang, Z. Ma, and R. Wang. An overview of phase change material slurries: MPCS and CHS. *Renewable and Sustainable Energy Reviews*, 14:598–614, 2010.

[81] F. Takeuchi, R. Ohmura, and K. Yasuoka. Statistical-thermodynamics modeling of clathrate-hydrate-forming systems suitable as working media of a hydrate-based refrigeration system. *Int. J. Thermophys*, 30:1838–1852, 2009.

[82] A. Delahaye, L. Fournaison, S. Marinhas, and M. Martínez. Rheological study of CO_2 hydrate slurry in a dynamic loop applied to secondary refrigeration. *Chemical Engineering Science*, 63:3551–3559, 2008.

[83] X. Wang and M. Dennis. An experimental study on the formation behavior of single and binary hydrates of TBAB, TBAF and TBPB for cold storage air conditioning applications. *Chemical Engineering Science*, 137:938–946, 2015.

[84] E. Hammerschmidt. Formation of gas hydrates in natural gas transmission lines. *Ind. Eng. Chem.*, 26(8):851–855, 1934.

[85] P. Brewer. Gas hydrates and global climate change. *Annals New York Academy of Sciences*, 912:195–199, 2000.

[86] D. Wuebbles and K. Hayhoe. Atmospheric methane and global change. *Earth-Science Reviews*, 57:177–210, 2002.

[87] E. Webb, P. Rensing, C. Koh, E. Sloan, A. Sum, and M. Liberatore. High-pressure rheology of hydrate slurries formed from water-in-oil emulsions. *Energy & Fuels*, 26:3504–3509, 2012.

[88] E. Webb, C. Koh, and M. Liberatore. High pressure rheology of hydrate slurries formed from water-in-mineral oil emulsions. *Ind. Eng. Chem. Res.*, 53(17), 6998-7007 2014.

[89] Y. Zhang, P. Debenedetti, R. Prud'homme, and B. Pethica. Differential scanning calorimetry studies of clathrate hydrate formation. *J. Phys. Chem. B*, 108:16717–16722, 2004.

[90] C. Lo, J. Zhang, S. Lu, A. Couzis, and J. Lee. Adsorption of surfactants on two different hydrates. *Langmuir*, 24(22):12723–12726, 2008.

[91] R. Wu, Z. Aman, E. May, K. Kozielski, P. Hartley, N. Maeda, and A. Sum. Effect of kinetic hydrate inhibitor polyvinylcaprolactam on cyclopentane hydrate cohesion forces and growth. *Energy & Fuels*, 28:3632–3637, 2014.

[92] B. Lee, C. Koh, and A. Sum. Mechanism of cohesive forces of cyclopentane hydrates with and without thermodynamic inhibitors. *Industrial and Engineering Chemistry Research*, 53:18189–18193, 2014.

[93] A. Ahuja, G. Zylyftari, and J Morris. Yield stress measurements of cyclopentane hydrate slurry. *Journal of Non-Newtonian Fluid Mechanics*, 220:116–125, 2015.

[94] P. Karanjkar, A. Ahuja, G. Zylyftari, J. Lee, and J. Morris. Rheology of cyclopentane hydrate slurry in a model oil-continuous emulsion. *Rheol Acta*, 55:235–243, 2016.

[95] P. Karanjkar, J. Lee, and J. Morris. Surfactant effects on hydrate crystallization at the water-oil interface: Hollow-conical crystals. *Crystal Growth & Design*, 12:3817–3824, 2012.

[96] D. Corak, T. Barth, S. Hoiland, T. Skodvin, R. Larsen, and T. Skjetne. Effect of subcooling and amount of hydrate former on formation of cyclopentane hydrates in brine. *Desalination*, 278(1-3):268–274, 2011.

[97] M. Nakajima, R. Ohmura, and Y. Mori. lathrate hydrate formation from cyclopentane-in-water emulsions. *Ind. Eng. Chem. Res.*, 47:8933–8939, 2008.

[98] B. Tohidi, A. Danesh, A. Todd, R. Burgass, and K. Østergaard. Equilibrium data and thermodynamic modelling of cyclopentane and neopentane hydrates. *Fluid Phase Equilibria*, 138(1-2):241–250, 1997.

[99] S. Fan, D. Liang, and K. Guo. Hydrate equilibrium conditions for cyclopentane and a quaternary cyclopentane-rich mixture. *J. Chem. Eng. Data*, 46(4):930–932, 2001.

[100] P. H. de Lima Silva. *Caracterização de emulsões de água em óleo visando ao estudo da formação de hidratos*. PhD thesis, Pontifícia Universidade Católica do Ro de Janeiro, 2014.

[101] A. Stender. *Reologia de Hidratos em emulsões de água-em-óleo na presença de ciclopentano*. PhD thesis, Pontifícia Universidade Católica do Ro de Janeiro, 2015.

[102] M. Barçante. *Estudo de emulsões de água em óleo para formação de hidratos*. PhD thesis, Pontifícia Universidade Católica do Ro de Janeiro, 2016.

[103] J. Nicholas, L. Dieker, E. Sloan, and C. Koh. Assessing the feasibility of hydrate deposition on pipeline walls—adhesion force measurements of clathrate hydrate particles on carbon steel. *Journal of Colloid and Interface Science*, 331:322–328, 2009.

[104] B. Leopércio, P. de Souza Mendes, and G. Fuller. Growth kinetics and mechanics of hydrate films by interfacial rheology. *Langmuir*, 32(17):4203–4209, 2016.

[105] G. Zylyftari, J. Lee, and J. Morris. Salt effects on thermodynamic and rheological properties of hydrate forming emulsions. *Chemical Engineering Science*, 95:148–160, 2013.

[106] A. Ahuja, G. Zylyftari, and J. Morris. Calorimetric and rheological studies on cyclopentane hydrate- forming water-in-kerosene emulsions. *Journal of Chemical & Engineering Data*, 60(2):362–368, 2015.

[107] R. Thompson, A. Alicke, and P. de Souza Mendes. Model-based material functions for SAOS and LAOS analyses. *Journal of Non-Newtonian Fluid Mechanics*, 215:19–30, 2015.

A
Details on the correction of the moduli

A.1
Constitutive models and SAOStrain analysis

The behavior of any material can be well represented by material functions associated to a constitutive model which must possess the same qualitative mechanical behavior as the material. The two most primitive models are the Hookean, for a purely elastic behavior, and the Newtonian, for a purely liquid behavior. From these models, two rheological parameters arise: the shear modulus (G) and the shear viscosity (η), defined in eqs. (1) and (2) respectively, as functions of the stress σ, strain γ and strain rate $\dot{\gamma}$ [107].

$$G = \frac{\sigma}{\gamma} \tag{1}$$

$$\eta = \frac{\sigma}{\dot{\gamma}} \tag{2}$$

For more complex materials - such as viscoelastic fluids or viscoplastic solids - a more elaborate constitutive model is required to perform better as a framework to interpret rheological data of complex materials. A very comprehensive explanation of the possible models and how to suitably choose one of them is given by Thompson et al. in ref. [107]. Here, only the Kelvin-Voigt model is briefly enlightened.

The Kelvin-Voigt model arranges the Hookean and the Newtonian mechanisms into a single model. Thereby, it represents a material that can sustain a nonzero constant shear stress while in static equilibrium. Thus, this model has both an associated shear modulus as well as an associated viscosity (eq. (3)). This arises from the assumption that there are two additive terms that compose the total stress σ: the elastic stress $\sigma_e = G\gamma$ and the viscous stress $\sigma_v = \eta\dot{\gamma}$. Consequently, the total strain is equal to the elastic strain and to the viscous strain: $\gamma = \gamma_e = \gamma_v$. As well, the total strain rate is equal to the elastic strain rate and to the viscous strain rate: $\dot{\gamma} = \dot{\gamma}_e = \dot{\gamma}_v$.

$$\sigma = G\gamma + \eta\dot{\gamma} \tag{3}$$

In small amplitude oscillatory strain flow (SAOStrain) analysis, where a sinusoidal strain wave of the form

$$\gamma(t) = \gamma_a \sin \omega t \quad \Rightarrow \quad \dot{\gamma}(t) = \gamma_a \omega \cos \omega t \tag{4}$$

is imposed, the strain amplitude γ_a and the strain rate amplitude $\gamma_a\omega$ are kept very small to ensure linearity. In this case, the classic storage and loss moduli G' and G'', defined by eq. (5), are the material functions.

$$\sigma = G'\gamma + \frac{G''}{\omega}\dot{\gamma} = \gamma_a G' \sin(\omega t) + G'' \cos(\omega t) \tag{5}$$

The Kelvin-Voigt framework is implicitly adopt in this analysis, meaning that the Kelvin-Voigt shear modulus and the Kelvin-Voigt viscosity are converted into material functions related to the classic moduli through

$$G = G' \quad \text{and} \quad \eta = G''/\omega. \tag{6}$$

A.2 The correction

Ring geometries for interfacial measurements are usually very delicate and can be easily deformed or broken. The correction presented here accounts for the additional strain due to the torsional load on the ring during experiments. As said in Section 3.4, this torque deforms the long and slender rods holding the ring itself (as illustrated in Fig. A.1) and this is not accounted for in the rheometer output. The intention is to determine the correct storage and loss moduli (G' and G'') of the interface tested, that do not depend on the geometry used.

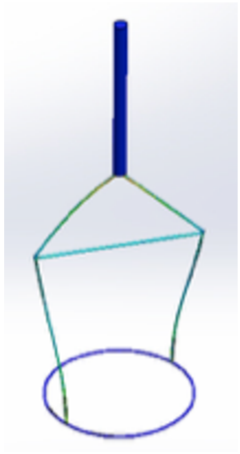

Figure A.1: Overstated simulation of how deformed the du Nouy ring can be during measurements.

The correction is based on the analog given in Fig. A.2, that represents the entire assembly. The geometry is assumed to be a perfectly elastic solid and is represented by the spring, with a correspondent shear modulus (G_r), based on the

Hookean model. The Kelvin-Voigt model is adopted for the interface. Thus, the interface is represented by a purely viscous damper and a purely elastic spring connected in parallel. The damper has a retardation viscosity associated to it (η) and the spring, a shear modulus (G).

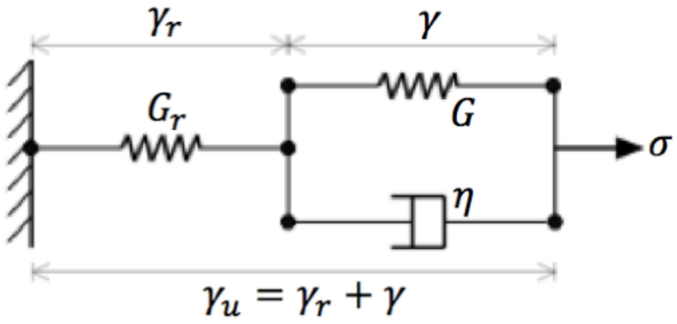

Figure A.2: The mechanical analog.

Thus, the total strain (γ_u) is obtained by adding the strain of the two springs: γ_r, for the ring, and γ, for the interface:

$$\gamma_u = \gamma_r + \gamma$$
$$\gamma_u = \frac{\sigma}{G_r} + \frac{\sigma - \eta\dot{\gamma}}{G}$$
$$\gamma_u = \frac{\sigma}{G_r} + \frac{\sigma}{G} - \frac{\eta}{G}(\dot{\gamma}_u - \dot{\gamma}_r)$$
$$\gamma_u = \frac{\sigma}{G_r} + \frac{\sigma}{G} - \frac{\eta}{G}\left(\dot{\gamma}_u - \frac{\dot{\sigma}}{G_r}\right)$$
$$\gamma_u = \left(\frac{1}{G_r} + \frac{1}{G}\right)\sigma - \frac{\eta}{G}\dot{\gamma}_u + \frac{\eta}{G_r G}\dot{\sigma}$$
$$\gamma_u = \frac{G_r + G}{G_r G}\sigma - \frac{\eta}{G}\dot{\gamma}_u + \frac{\eta}{G_r G}\dot{\sigma}$$

Now, it is possible to rearrange to separate strain and stress:

$$\sigma + \frac{\eta}{G_r + G}\dot{\sigma} = \frac{G_r G}{G_r + G}\gamma_u + \frac{\eta G_r}{G_r + G}\dot{\gamma}_u \tag{7}$$

Substituting eq. (6) in (7), where G' and G'' are the unknowns storage and loss moduli of the interface, respectively:

$$\sigma + \frac{G''}{\omega(G_r + G')}\dot{\sigma} = \frac{G_r G'}{G_r + G'}\gamma_u + \frac{G'' G_r}{\omega(G_r + G')}\dot{\gamma}_u \tag{8}$$

Choosing the Kelvin-Voigt framework for the entire assembly also, the stress will be of the form

$$\sigma(t) = \gamma_a G'_u \sin\omega t + \gamma_a G''_u \cos\omega t \quad \Rightarrow \quad \dot{\sigma}(t) = \gamma_a \omega G'_u \cos\omega t - \gamma_a \omega G''_u \sin\omega t \quad (9)$$

where G'_u and G''_u are the uncorrected storage modulus and loss modulus of the assembly, measured by the rheometer.

We now plug eqs. (4) and (9) into eq. (8) and collect the terms multiplied by $\sin\omega t$ and the ones multiplied by $\cos\omega t$:

$$\left[G'_u - \frac{G''G'_u}{G_r + G'} - \frac{G_r G'}{G_r + G'}\right]\sin\omega t + \left[G''_u - \frac{G''G'_u}{G_r + G'} - \frac{G_r G''}{G_r + G'}\right]\cos\omega t = 0 \quad (10)$$

Since eq. (10) is valid for all t's, then both terms between square brackets must be null. This gives us two equations for the two unknowns G' and G'':

$$G' = \frac{G_r G'_u(G_r - G'_u) - G''^2_u}{G'^2_u + G''^2_u + G_r(G_r - 2G'_u)} \quad (11)$$

and

$$G'' = \frac{(G_r + G')G''_u}{G_r - G'_u}$$

or

$$G'' = \frac{G_r G''_u}{G_r - G'_u} + \frac{G''_u}{G_r - G'_u}\left(\frac{G_r G'_u(G_r - G'_u) - G''^2_u}{G'^2_u + G''^2_u + G_r(G_r - 2G'_u)}\right) \quad (12)$$

where G_r is the effective shear modulus of the ring, previously measured (see Sec. A.3), and G'_u and G''_u are the storage and loss moduli of the assembly, supplied by the rheometer.

Fig. A.3 presents the comparison between the uncorrected (G'_u and G''_u) and the corrected (G' and G''), in blue and red respectively. The filled symbols indicate the storage moduli while the empty symbols indicate the loss moduli.

The importance of the correction is clear once it shifts the moduli curves to higher values. The difference between the uncorrected and the corrected moduli increases with time which corresponds to the hydrate film evolution. Thus, the greatest difference occurs at the end of the test, when the hydrate film is more well constituted. It makes sense once the rods holding the ring deform more when it is completely attached to the hydrate structure.

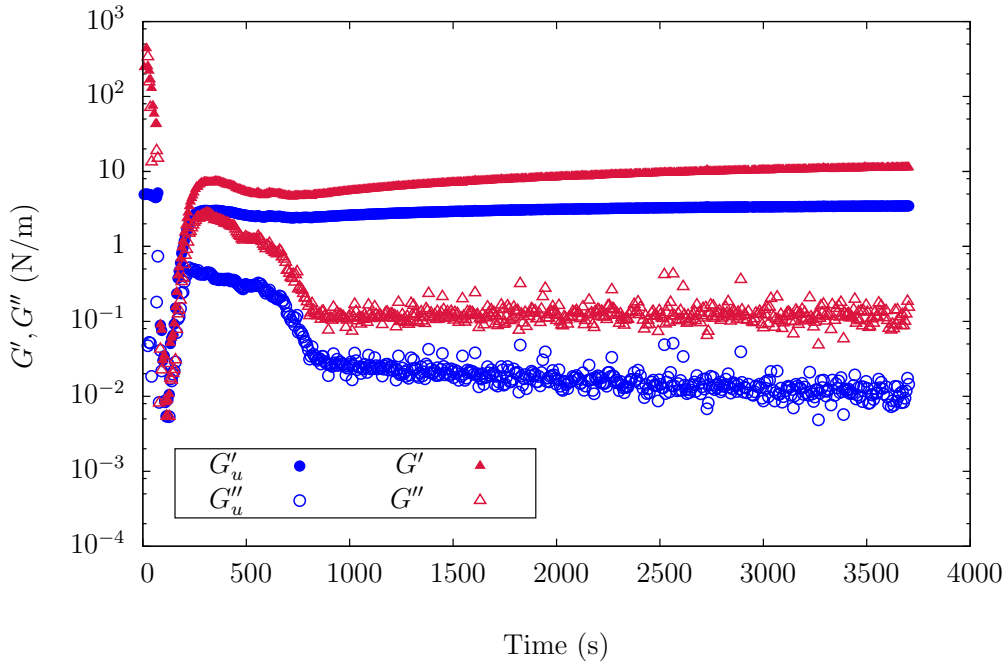

Figure A.3: Time sweep: comparison between uncorrected and corrected curves.

Note that G_r is defined for any ring. In Chapter 3 (Sec. 3.4), G_r corresponds to the du Nouy ring effective shear modulus. It can be measured following the procedure presented in next section (Sec. A.3). In case of tests using another ring geometry (e.g. the Double Wall Ring), its shear modulus should be measured and taken into account.

It is not difficult to see that, in the limit $G_r \to \infty$, eqs. (11) and (12) give $G' = G'_u$ and $G'' = G''_u$. Moreover, the expression obtained assuming that the material is also a perfectly elastic solid, namely $G' = G'_u G_r/(G_r - G'_u)$, is obtained by setting $G'' = 0$ in the first term between square brackets of eq. (10).

A.3
Measuring the effective shear modulus of the ring, G_r

The effective shear modulus of the ring can be measured in a rheometric experiment in which a torque is applied to the geometry whose ring is completely attached to the interface. Thus, the rods of the ring can deform but the "interface" remains static. To simulate this ideal condition, we built a very simple brass device, shown in Fig. A.4, that holds the ring and impedes its movement.

Figure A.4: Brass device for G_r measurement.

Fig. A.5 illustrates the step by step procedure to assemble the apparatus. The device is placed on top of the Peltier plate. Then, the ring is gently fitted in the circle in the middle of the device, touching its upper part. After that, an acrylic piece is used to hold the ring. Two screws fixe it firmly.

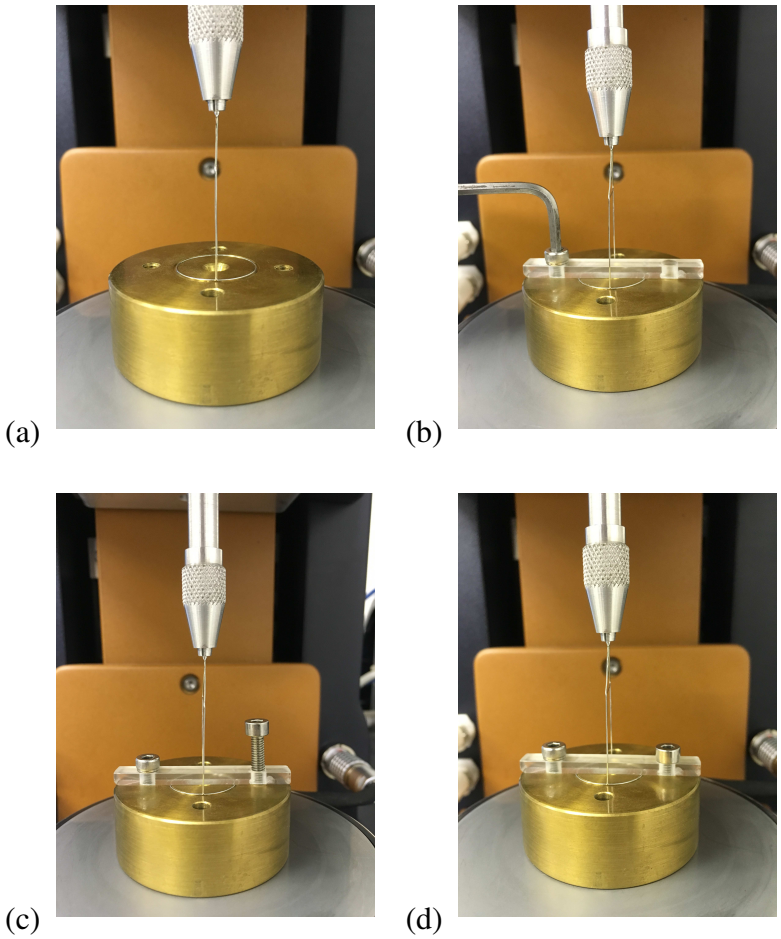

Figure A.5: Step by step procedure to assemble the brass device.

With this installation and because of the device weight (≈ 3kg), only the rods of the geometry deform when small torques are applied, accordingly to Fig. A.1. So,

a time sweep test can be set and the effective shear modulus of the ring geometry itself, measured.

For the du Nouy ring used in all the experiments reported in Chapter 4, the value measured was $G_r = 5\,\text{N/m}$. Notwithstanding, the same procedure can be adapted for different geometries. Besides, other methods can be adopted to measure the effective shear modulus of the ring.